



Assessing the potential of Individual Foraminifera Analyses ($\delta^{18}\text{O}$) to reconstruct variability, seasonality and extremes in the tropical Indian Ocean

Yohan Lichterfeld^{1*}, Guillaume Leduc¹, Kaustubh Thirumalai², Laurence Vidal¹, Thibault de Garidel-Thoron¹, Corinne Sonzogni¹, Clara T. Bolton¹

¹Aix-Marseille Univ, CNRS, IRD, INRAE, CEREGE, Aix-en-Provence, France

²Department of Geosciences, University of Arizona, 1040 E, 4th Street Tucson, AZ 85721, USA

*Correspondence to: Yohan Lichterfeld (lichterfeld@cerege.fr)

Abstract. The Indian Ocean plays a critical role in the global climate system by regulating heat and moisture transport, influencing major fluxes that drive atmospheric circulation. Individual foraminiferal analyses (IFA) of the stable oxygen isotope composition ($\delta^{18}\text{O}$) of their test provides a powerful approach to reconstruct past climate variability beyond changes in mean conditions, with the potential to capture seasonal to interannual climatic extremes associated with phenomena such as the Indian monsoon and the Indian Ocean Dipole (IOD). However, field-based calibrations of this proxy remain sparse in the Indian Ocean, especially in the western part of the basin, limiting our understanding of how IFA records regional hydrographic signals. In this study, we combine a forward-modelling approach with IFA in Indian ocean core-top sediment samples to evaluate how $\delta^{18}\text{O}$ variability responds to changes in temperature and salinity linked to seasonal and interannual variability. Using ocean reanalysis data, we simulate surface and thermocline conditions at several sites representative of different oceanographic provinces across the Indian Ocean and generate synthetic core-top IFA datasets through random sampling. We evaluate the sensitivity of results by artificially amplifying or reducing seasonal and interannual climate variability. Forward-modelled data are then compared with IFA data from core-tops at four key sites across the Indian Ocean. Our results show that surface-ocean individual foraminiferal $\delta^{18}\text{O}$ changes in the western and central Indian Ocean are mainly controlled by temperature seasonality related to monsoon dynamics, whereas in the eastern Indian Ocean, seasonality is less pronounced and interannual variability is more dominant. On the other hand, thermocline $\delta^{18}\text{O}$ variability for all sites is primarily associated with interannual variability and temperature changes, highlighting the potential of thermocline species to record interannual temperature variability. Forward-modelled IFA closely match real datasets from Late Holocene core-tops for surface and thermocline depths. This framework provides a basis for interpreting IFA in the Indian Ocean in terms of underlying climate processes and offers perspectives for reconstructing past seasonal and interannual climate variability in this important region.



30 1 Introduction

The evolution of climate variability at seasonal and interannual timescales plays a key role in shaping the occurrence and intensity of extreme weather events. In order to better understand the sensitivity of seasonal to interannual climate variability and its consequences on the hydrological cycle (Swain et al., 2025), it is essential to reconstruct variability at these timescales under climatic background conditions different from those observed during the instrumental period.

35 Seasonal to interannual sea surface temperature (SST) variability in the tropical oceans disrupts the global hydrological cycle, with strong repercussions for tropical countries (Rasmussen and Carpenter, 1982; Gadgil, 2003). Ocean-atmosphere interactions give rise to phenomena such as El Niño–Southern Oscillation (ENSO) in the equatorial Pacific Ocean and the Indian Ocean Dipole (IOD) in the tropical Indian Ocean. ENSO is the primary mode of interannual variability on Earth and leads to strong modifications in equatorial upwelling and easterlies. Whilst the IOD presents

40 relatively weaker variability than ENSO, it manifests on the eastern and western sides of the Indian Ocean basin (Saji et al., 1999). Its consequences for regional hydroclimate are profound, driving anomalous rainfall, drought, and flood events across East Africa, the Indian subcontinent, and Southeast Asia (Ummenhofer et al., 2009; Anderson et al., 2019), making it one of the most socially impactful climate mode in the world, affecting the livelihoods of over a billion people across the basin. IOD variability is mainly influenced by the equatorial SST gradient and the direction of prevailing

45 winds. On the seasonal timescale, due to its enclosed northern boundary, the northern Indian Ocean is under the influence of seasonally-reversing monsoon winds, with the southwest monsoon bringing high precipitation to southern Asia and the Bay of Bengal during boreal summer, and a drier northeast monsoon during boreal winter. The monsoon impacts the hydrological cycle and in situ populations living around the basin, causing extreme events.

50 Understanding the variability of the Indian Ocean climate and extreme events remains challenging, especially in the context of climate change. Future projections from modelling studies suggest that the Indian Ocean could harbor enhanced variability with more intense and frequent extreme events arising due to an intensified zonal SST gradient (Abram et al., 2008; Cai et al., 2013, 2014; Roxy et al., 2014; Zheng et al., 2013). Indeed, recent observations suggest that these changes are already significantly altering the hydrological cycle across the Indian Ocean basin (Ummenhofer et al., 2018). Yet, the future evolution

55 of rainfall dynamics at regional scales remains model-dependent, and their impact on hydrological cycle extremes may depend on how well the future evolution of Indo-Pacific SST variability is reproduced by climate models (Park et al., 2022). Documenting how large climate perturbations may have affected the magnitude and frequency of climate extremes in south to south-east Asia in the past could help evaluate the ability of climate models to reproduce the ocean-atmosphere interactions



60 that underpin climate extremes. To reconstruct past climate variability, individual planktonic foraminiferal analyses (IFA) are
a well-established technique that can provide such diagnostics under contrasting climate backgrounds (Fehrenbacher et al.
2024; Leduc et al. 2009). Traditional $\delta^{18}\text{O}$ paleoclimate analysis methods focus on reconstructing average climate conditions,
while IFA offers the advantage of recording the full climate spectrum within a time slice rather than mean climate. Due to low
(generally <5 cm/kyr) accumulation rates and bioturbation in open-ocean marine sediments, multi-test “bulk” foraminiferal
analyses cannot typically record seasonal or interannual climate signatures. Yet they contain interesting snapshots on total
65 variability that, once correctly calibrated with respect to regional ocean characteristics, can help decipher the mode of climate
variability that influenced the recorded changes in IFA variability. IFA has been applied in many studies to reconstruct past
modes of ENSO or IOD variability (Leduc et al., 2009; Ford et al., 2015; Thirumalai et al., 2019; 2024) and to capture monsoon
dynamics (Ganssen et al., 2011; Thirumalai and Clemens., 2020; Thirumalai et al., 2025).

70 The application and accurate interpretation of IFA in the Indian Ocean requires careful consideration to account for region-
specific climate, ocean dynamics, and foraminiferal ecology using modern datasets (Thirumalai et al., 2013; Bienzobas-
Montávez et al. 2019). In this study, we aim to understand how modern climatic and oceanographic variability in the Indian
Ocean is recorded by forward-modelling IFA- $\delta^{18}\text{O}$ and testing the sensitivity of this proxy using modern reanalysis datasets
(ORAS5). We do this at four distinct sites representative of distinct oceanographic provinces, in the northeastern, western,
75 central and eastern Indian Ocean (Fig. 1). Forward modelled data are then compared with new and published core-top (late
Holocene) IFA measurements performed on the planktonic species *Globigerinoides ruber* and *Neogloboquadrina dutertrei*, to
constrain surface and thermocline variability, respectively. In this study, we will discuss the applicability of IFA to reconstruct
variability and extremes in the Indian Ocean in three steps. (1) Describe seasonal and interannual variability patterns in the
surface and thermocline based on reanalysis in our key areas; (2) Illustrate how an increase in seasonality and interannual
80 variability would manifest itself in modelled IFA by modifying these patterns based on reanalysis; and (3) Compare IFA
measured in real core-tops with forward-modelled IFA from the reanalysis.

2 Study sites and climatic setting of the tropical Indian Ocean

85 We focus on four sites distributed across the western and central tropical Indian Ocean to investigate the controls on planktonic
carbonate $\delta^{18}\text{O}$ ($\delta^{18}\text{O}_c$) variability using both IFA forward-modelling and measurements: International Ocean Discovery
Program (IODP) Site U1467 (73.17°E, 4.5°N, 487.4 m water depth), Site MD96-2060 (40.46°E, 8.30°S, 2026m), Site NIOP
905 (51.95°E, 10.76°N, 1575m) and Site SO189-39KL (99.90°E, 0.78°S, 517m) (Fig. 1). These sites span distinct
oceanographic settings influenced by different modes of variability and regional water-mass dynamics.



- 90 IODP Site U1467 (Maldives) is governed by the seasonal reversal of monsoonal winds under the strong influence of the south Asian monsoon system (Wang et al., 2005). These wind reversals strongly modulate surface ocean currents, SST, salinity, and upwelling intensity in the western Arabian Sea. During boreal summer, strong southwesterlies winds drive the eastward-flowing Summer Monsoon Current. In contrast, during boreal winter, the Winter Monsoon Current flows westward, transporting low-salinity waters from the Bay of Bengal to the Arabian Sea (Fousiya et al., 2016; Behara et al., 2016).
- 95 Thermocline depth is highly sensitive to IOD phases especially in the western Indian ocean, shoaling during negative events and deepening during positive years (Sankar et al., 2021).

Site NIOP 905 (Somali Margin) is located in the most intense upwelling system in the Indian Ocean. The upwelling system is primarily driven by the Somali Jet during the southwest (summer) monsoon, which enhances alongshore winds off Oman and induces coastal and offshore upwelling via Ekman transport and the Somali coastal current (Schott and McCreary, 2001; Hood et al., 2017). During the northeast monsoon, upwelling is reduced promoting higher SST (Izumo et al., 2008), leading to high seasonality in SST (9-11°C) during a year. As compared to other sites, this site is most affected by upwelling, with intense primary productivity occurring during most of the year culminating during summer (Wiggert et al., 2005) and a shallower thermocline depth.

105 Site MD96-2060 offshore Tanzania, lies within the East African Coastal Current (EACC). The EACC exhibits clear seasonal modulation by monsoonal winds: it strengthens during the southwest monsoon (April–September) and weakens during the northeast monsoon months (November–February) (Mayorga-Adame et al., 2016; Vinayachandran et al., 2021). Thermocline temperatures exhibit a seasonal range of ~1–2°C.

110 Site SO189-39KL, located in the eastern Indian Ocean, is situated within the Sumatra coastal upwelling system, which exhibits strong seasonal intensification during the southwest monsoon (Susanto et al., 2001). Seasonal variability in SST and Sea surface salinity (SSS) is nonetheless recorded and is controlled by the migration of the Intertropical Convergence Zone (ITCZ), not by the monsoon or by ENSO directly (Aldrian and Susanto, 2003). Within the thermocline, temperature fluctuations are

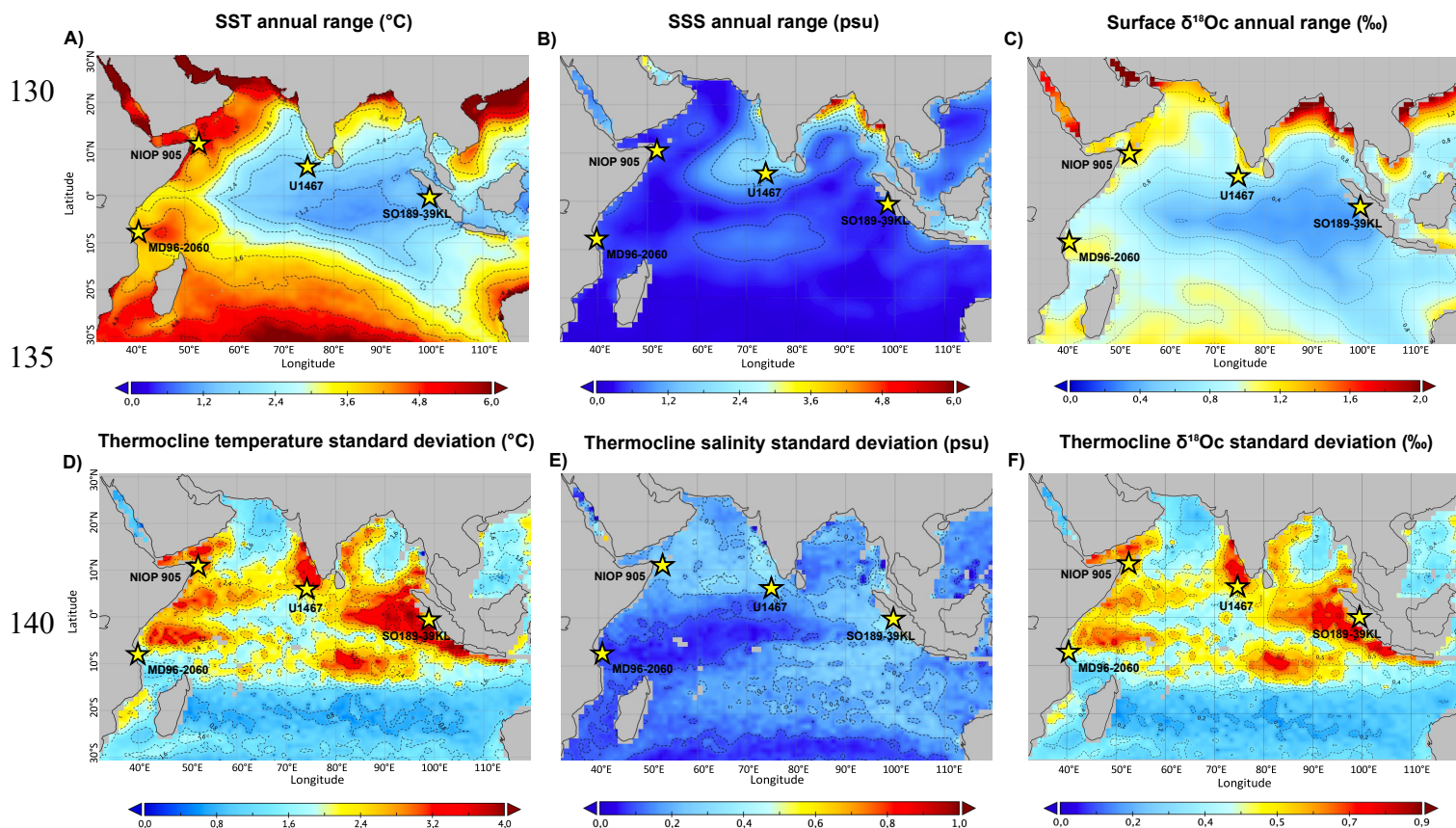
115 mainly influenced by IOD events (Yu et al., 2005, Qiu et al., 2012).

Together, these sites provide a comprehensive view of the spatial heterogeneity of Indian Ocean variability, encompassing monsoon-dominated northern regions, the western boundary current system, and the IOD and upwelling-influenced eastern equatorial zone. Their contrasting oceanographic settings allow us to test the sensitivity of $\delta^{18}\text{O}_c$ variability to seasonal and

120 interannual forcing and to evaluate the performance of IFA forward-modelling across diverse climatic regimes.



125



135

140

Figure 1. Modern seasonality in SST and SSS, and estimated $\delta^{18}O_c$ in the tropical Indian Ocean at surface and thermocline depths. (A-C) Annual range of sea surface temperature (SST), sea surface salinity (SSS), and $\delta^{18}O_c$ at the surface (top row). (D-F) Annual standard deviation of temperature, salinity and $\delta^{18}O_c$ for thermocline depth. Calculations were performed based on the ORAS5 reanalysis dataset from 1958 to 2018.

150



3 Methods

3.1 Forward-modelling of planktonic IFA $\delta^{18}\text{O}_c$

155 3.1.1 Calculating surface and thermocline $\delta^{18}\text{O}_c$ time series from ocean reanalysis

To simulate $\delta^{18}\text{O}_c$ variability at the selected sites, we used the ORAS5 ocean reanalysis dataset, which provides monthly fields of temperature and salinity at 1° resolution for the period 1958–2018. For each site, we extracted time series at two depths representative of the surface mixed-layer and thermocline conditions the Indian Ocean (Fig. 2A): 0.5 m for surface conditions, and 97 m for the thermocline for all sites. The choice of 97 m for thermocline depth was made based on available depths in the ORAS5 analysis dataset, and which of these most closely matched the depth of the highest SD extracted from temperature profiles at our four sites ($\sim 100\text{m}$ depth; Fig. 2B). Depth profiles of temperature and salinity show similar thermocline depths for all four sites, despite being influenced by contrasting oceanographical regimes (Fig. 2A).

160

Simulated $\delta^{18}\text{O}_c$ values were computed based on the paleotemperature equation of Bemis et al. (1998) applied under low-light conditions. The corresponding $\delta^{18}\text{O}$ sea water ($\delta^{18}\text{O}_w$) values were estimated from salinity using depth-specific $\delta^{18}\text{O}_w$ –S relationships. For the surface, we chose to apply the same equation for all sites to produce comparable changes under an altered climate. We applied the equation of Thirumalai and Clemens (2020), which has been adapted from Singh et al. (2010), which is similar to the $\delta^{18}\text{O}_w$ –S relationships commonly found in tropical surface waters (Schmidt et al., 2007) (Eq. (1)):

165

$$\text{Surface: } \delta^{18}\text{O}_w = 0.26 * S - 8 \quad (1)$$

For the subsurface (70–120 m), we derived a new relationship based on the global dataset of LeGrande and Schmidt (2006), restricted to this depth range (Fig. S1) (Eq. (2)):

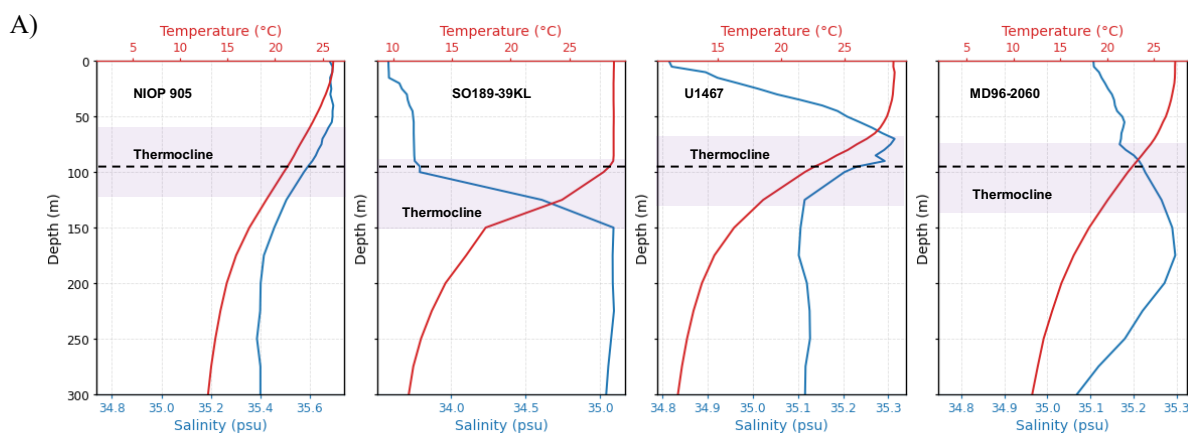
170

$$\text{Thermocline: } \delta^{18}\text{O}_w = 0.45 * S - 15.43 \quad (2)$$

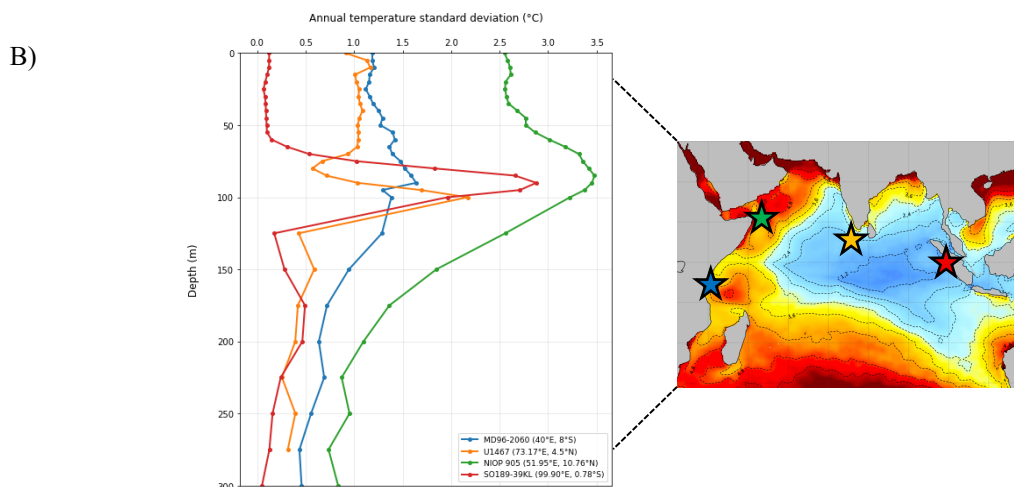
175



180



185



190 **Figure 2.** Modern vertical oceanographic profiles and temperature variability at the four study sites. Top panels: Mean vertical profiles of
 191 temperature (red) and salinity (blue) for each site. The shaded area indicates the depth range of the thermocline (defined on the increase of
 192 temperature gradient). Bottom panel: Temperature standard deviation (°C) versus depth (0–300 m) derived from WOA23 (World Ocean
 193 Atlas) with the location of the sites represented by coloured stars.

3.1.2 Simulating synthetic planktonic foraminifera IFA core-tops

195 The temperature and salinity timeseries extracted from ORAS5 are used to identify how increasing variability will be imprinted
 196 in the surface and subsurface Indian Ocean when the corresponding $\delta^{18}\text{O}_c$ values are calculated. We therefore opted to use a
 197 constant $\delta^{18}\text{O}_w$ -S relationship to better illustrate how modifying seasonal and interannual temperature and salinity values would
 198 affect an idealized, continuous synthetic $\delta^{18}\text{O}_c$ timeseries. However, for the simulation of synthetic IFA data, to allow for direct
 199 comparison with measured data from the same locations, we use region-specific $\delta^{18}\text{O}_w$ -S relationships, as applied in the
 200 original publications when available, or calculated from Delaygue et al. (2001).



205 Based on the modelled surface and thermocline $\delta^{18}\text{O}_c$ timeseries using the ORAS5 monthly reanalysis data for any coordinate and depth, we carried out random IFA sampling (60 individuals) across the 1958–2018 period (720 months) following the procedure of Thirumalai et al. (2013). Each individual foraminifera is assumed to record the average monthly environmental conditions of its calcification period. By sampling randomly throughout the 60-year timeseries, we simulate a continuous and
210 constant shell flux, effectively integrating the climatic signal while avoiding any assumption of a seasonally phase-locked life cycle that is, we do not prescribe a fixed monthly calcification window tied to the reanalysis calendar. To assess the influence of altered climate variability on $\delta^{18}\text{O}_c$, we artificially increased (or decreased) the amplitude of seasonal variability in surface waters by $\pm 75\%$. This range of amplitude was selected as a sensitivity benchmark to simulate extreme monsoonal or IOD/ENSO regimes, consistent with the values used in a previous study (Thirumalai and Clemens., 2020). For the thermocline,
215 we modified the amplitude and frequency of interannual variability by injecting random events similar to potential IOD/ENSO events that create anomalies in which temperature and salinity are modified by $\pm 75\%$.

For each altered and original dataset, 60 values were randomly sampled to simulate an IFA-style core-top sampling with a statistically robust SD (Leduc et al., 2009). We applied a Monte-Carlo bootstrap procedure (1000 resampled iterations of 60 randomly selected individuals) to each dataset and scenario to ensure that altered conditions would be detectable. The
225 distribution of this ensemble of resampling do not overlap, implying that IFA is a method suitable to detect past changes in variability under contrasting climate conditions.

We finally evaluate the effect of these scenarios using Quantile–Quantile (Q–Q) plots, which jointly compare the distributions of $\delta^{18}\text{O}_c$ values of the original and altered datasets. Q–Q plots are useful for visualizing both systematic and non-linear deviations caused by changes in temperature and salinity. An alignment along the 1:1 reference is expected if two IFA
230 distributions are statistically the same. Any deviations from this line will reflect changes in the background (without changes in the slope), magnitude (alignment along a different slope) or with other recognizable structures of changing total variability, such as skewness (arcuate-shaped Q–Q plot). This method has already proven useful for visualizing how interannual variability was altered in previous IFA studies (Ford et al., 2015; Thirumalai et al., 2019).

3.2 IFA Measurements and Statistics

225 In this study, we present new measurements of IFA $\delta^{18}\text{O}$ in core-top samples (Late Holocene, 0–4 ka) from Sites MD96-2060, IODP U1467, and NIOP 905. We selected two species with distinct ecological niches (Chaabane et al., 2026): *Globigerinoides ruber* is a surface-dwelling, symbiont-bearing species that calcifies throughout the year within the upper mixed layer (Fairbanks et al., 1982; Stainbank et al., 2019) and *Neogloboquadrina dutertrei* is a thermocline-dwelling species commonly found in the deep chlorophyll maximum (DCM), associated with the pycnocline (Chaabane et al., 2026 ; Kemle-von Mücke
230 and Oberhänsli., 1999). *N. dutertrei* is particularly useful in reconstructions of interannual variability, due to its sensitivity to thermocline depth changes linked to phenomena such as ENSO and IOD (Leduc et al., 2009; Thirumalai et al., 2013; Ford et



al., 2015). New $\delta^{18}\text{O}$ data are measured on *G. ruber* and *N. dutertrei* for site MD96-2060, *N. dutertrei* for site U1467 and *N. dutertrei* for site NIOP 905 (Table 1). We also use published *G. ruber* data from Site NIOP 905 (Ganssen et al., 2011) and IODP Site U1467 (Stainbank et al., 2020).

235 Planktonic foraminifera were picked from the 215–315 μm size range. New $\delta^{18}\text{O}$ c analyses were conducted using a Thermo-Finnigan Delta V-Plus IRMS coupled with a Carbo-Kiel IV carbonate preparation device at CEREGE. The international standard NBS-19 was used for calibration, and $\delta^{18}\text{O}$ values are reported in per mil (‰) relative to the Vienna Pee Dee Belemnite (VPDB) standard. The mean external reproducibility (1σ) was better than 0.08 ‰ for $\delta^{18}\text{O}$.

240 To assess the similarity between the IFA distributions observed in core-tops and those generated by forward-modelling, we applied several statistical tests. These included assessments of normality (e.g., Shapiro-Wilk), and comparisons of the means, SD, and distribution (skewness, kurtosis). Classical significance tests were also applied to assess whether differences between datasets (modelled vs. measured) were statistically significant. Outliers were identified using the interquartile range (IQR) method, as data that fall outside the 95% of the distribution bounded by $Q1 - 1.5 * \text{IQR}$ and $Q3 + 1.5 * \text{IQR}$, where $\text{IQR} = Q3 - Q1$. This method has been successfully applied in Ganssen et al., (2011) on core NIOP 905, and only 5 individual analyses
 245 among a total of 139 measurements for the newly generated IFA data were identified as outliers (Fig. S2). Those outliers are flagged later in Chapter 5 and do not alter the evaluation of the sedimentary core-top. Core-tops dating and age models applied are reported in Table 1 and described in Ivanochko et al. (2005) for NIOP 905, Mohtadi et al. (2010, 2011, 2014) for SO189-39KL and Stainbank et al. (2020) for Site U1467, and Dauvier et al., (submitted) for MD96-2060 (Table 1).

Site	Latitude / Longitude	Water Depth (m)	Core-top age (kyr)	Reference Age	$\delta^{18}\text{O}$ -IFA <i>G. ruber</i> data	$\delta^{18}\text{O}$ -IFA <i>N. dutertrei</i> data
NIOP 905	10.76N, 51.95E	1575	0.95	Ivanochko et al., 2005	Ganssen et al., 2011	This study
U1467	4.51N, 73.17E	487.4	0.1	Stainbank et al., 2020	Stainbank et al., 2019	This study
SO189-39KL	0.78S, 99.9E	517.0	0.41	Mohtadi et al., 2014	Thirumalai et al., 2019	No data
MD96-2060	8.3S, 40.46E	2026	3.9	Dauvier et al., 2026 (submitted)	This study	This study

Table 1. Summary of core-top sediment sites and associated Individual Foraminifera Analysis (IFA) datasets. Location (latitude/longitude), water depth, and age models for the four study sites are provided along with the corresponding references. The table specifies whether the $\delta^{18}\text{O}$ -IFA data for the surface-dwelling species *G. ruber* and the thermocline-dwelling species *N. dutertrei* are newly generated for this study
 260 or sourced from previous publications.



265 A critical consideration in interpreting IFA variability is the potential for dissolution of the calcite tests analysed. First, the bathymetric setting of the cores ranging from 487 m at Site U1467 to 2026 m at Site MD96-2060 places all samples well above the modern Indian Ocean lysocline, typically situated between 3500 and 3800 m (Feely et al., 2004; Peterson and Prell., 1985). Second, visual inspection of *G. ruber* and *N. dutertrei* tests reveals good preservation. Consequently, we conclude that the observed IFA distributions represent primary climate signals rather than a signature of differential preservation across the varying water depths of the sites that would lead to difference in homogenisation and altered variability.

4 Results

270 4.1 Forward modelled synthetic time-series and IFA core-top $\delta^{18}\text{O}_c$ under modern conditions

4.1.1 Time series extracted from reanalysis dataset

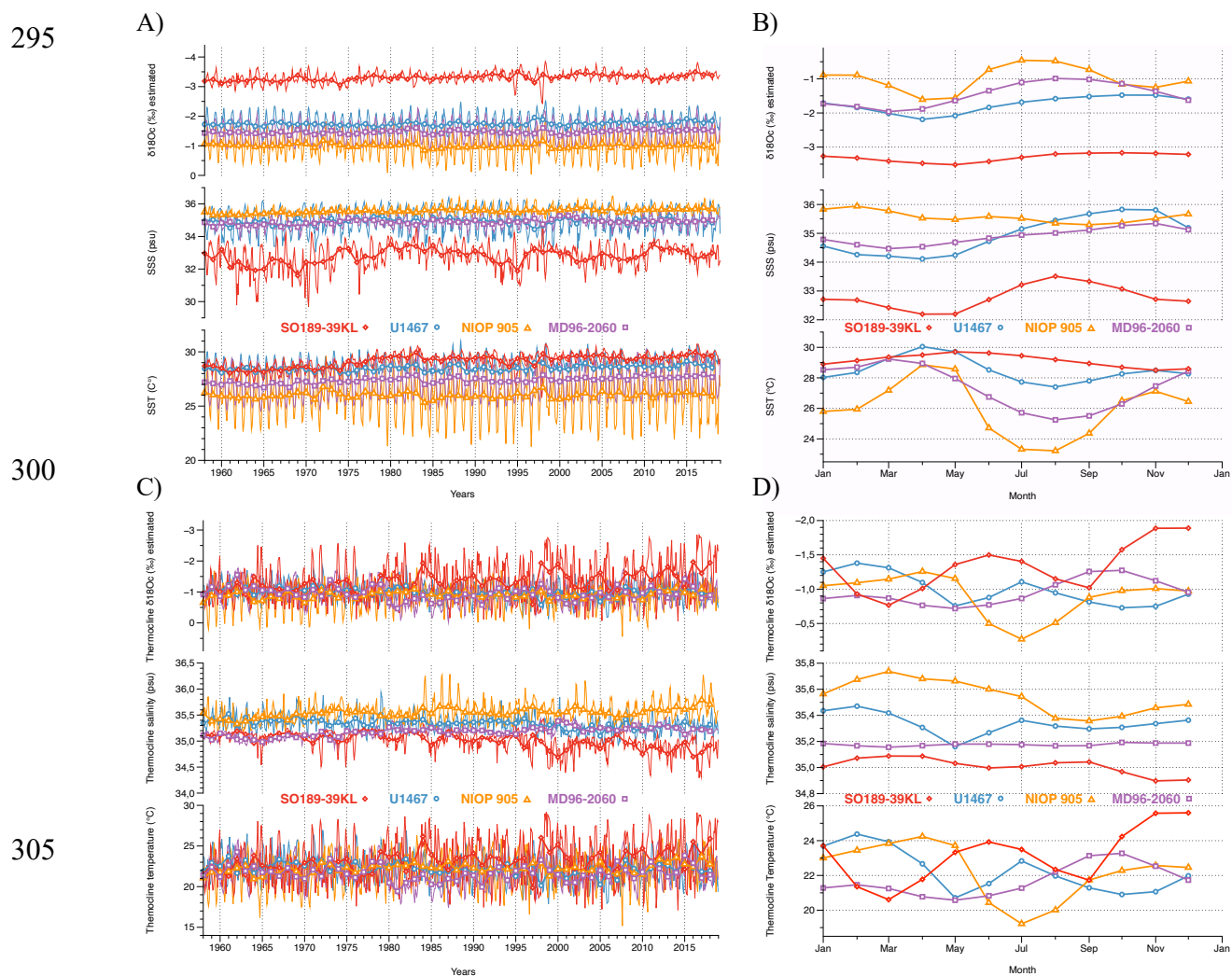
275 At the seasonal timescale, SST exhibits the highest variability at sites NIOP 905 and MD96-2060, with SST amplitude ranging from 23°C in boreal summer to 29°C in spring and 25°C in summer to 29°C in spring, respectively. In contrast, the other two sites show a weaker SST seasonality, with Site U1467 showing seasonal variability of 2–3°C and SO189-39KL less than 1°C (Fig. 3B). Seasonal SSS variability is relatively low for Sites MD96-2060 and NIOP 905 (<1 psu), and higher for Sites SO189-39KL (1.5 psu) and U1467 (2 psu) (Fig. 3B). These variabilities translate into a modelled $\delta^{18}\text{O}_c$ variability that increases in line with SST seasonality, exhibiting maximum amplitude of 1.5‰ at Site NIOP 905. Only the eastern Indian Ocean site shows seasonal surface $\delta^{18}\text{O}_c$ variability of less than 0.5‰.

280 SST and $\delta^{18}\text{O}_c$ variability are higher at the seasonal scale for the surface than the thermocline for all sites. Overall, results highlight that the drivers of surface $\delta^{18}\text{O}_c$ are mainly related to temperature variability in the western basin. Whereas salinity becomes more significant for the Maldives and in the east. Interannual variability at the surface is relatively low (<1.5°C in SST and <1 psu in SSS), resulting in $\delta^{18}\text{O}_c$ fluctuations that do not exceed 0.5‰. Maximum interannual variability is observed at eastern Indian Ocean Site SO189-39KL (Fig. 3B). At most of the sites, surface water variability is mainly driven by seasonal variability and theoretically the most sizeable interannual signal is found within the thermocline where we find the highest temperature SD values (Fig. 2).

Interannual thermocline (97m) temperatures at interannual timescale (thick curves on Fig. 3C) show the strongest amplitudes at sites MD96-2060 (4.8°C) and SO189-39KL (6.3°C), whereas Sites U1467 and NIOP 905 display lower amplitudes (3.6°C and 2.7°C). Salinity at thermocline depth varies between 0.2 and 0.5 psu at all sites, with a slightly higher amplitude (0.52 psu) at Site SO189-39KL. The simulated thermocline $\delta^{18}\text{O}_c$ exhibits a maximum amplitude of 1‰ at MD96-2060 and 1.3‰ at



290 SO189-39KL, followed by 0.64‰ at U1467 and 0.48‰ at NIOP 905. This indicates that sites SO189-39KL (east) and MD96-
 2060 (west) are the most sensitive to interannual thermocline variability. At the seasonal timescale (thin curves, Fig. 3D), the
 maximum amplitudes are found in sites NIOP 905 and SO189-39KL. Over the instrumental period (1958–2018), the
 superposition of interannual variability on the seasonal cycle increases the temperatures range to 11°C at site NIOP 905. This
 strong total variability results in a calculated $\delta^{18}\text{O}_c$ amplitude of up to 2.78‰.



300
 305
Figure 3. Modern surface and subsurface (thermocline) variability at the four studied sites (U1467, NIOP 905, MD96-2060 and SO189-
 310 39KL), derived from ORAS5 reanalysis datasets (1958–2018). A) and C): Monthly time series of $\delta^{18}\text{O}_c$, salinity, and temperature at both
 the surface (top) and thermocline depth (bottom). B) and D) The right panels show the corresponding monthly mean values (averages for
 each month over the 1958–2018 period) for each variable.



315 At all sites, modern climatology data show that seasonal variations dominate in the surface ocean, with relatively lower-
amplitude interannual timescale variability (Fig. 3A). At the depth of the thermocline, all sites show increased sensitivity to
interannual variability relative to at the surface (Fig. 3C). Site SO189-39KL shows the strongest interannual variability in
temperature (and therefore in modelled $\delta^{18}\text{O}_c$), followed by site MD96-2060. At sites NIOP 905 and U1467, thermocline
variability on interannual timescales is more muted, and seasonal variations in SST and SSS at thermocline depths are larger
320 (Fig. 3D). These variations are interpreted in the discussion below by linking our data with modes of variability and measured
 $\delta^{18}\text{O}$ -IFA.

4.1.2 Artificial modern amplification of seasonal and interannual variability and its effect on forward-modelled IFA

325 The temporal evolution of the calculated $\delta^{18}\text{O}_c$ from the reanalysis datasets (1958–2018) illustrates the theoretical proxy
response to an increase in high-frequency variability by 75% (Fig. 4). For each site, we compare temperature, salinity and
 $\delta^{18}\text{O}_c$ timeseries of ORAS5 (blue curve), and the altered timeseries scenario (red curve), where seasonal or interannual
variability was artificially amplified or reduced to test IFA sensitivity.

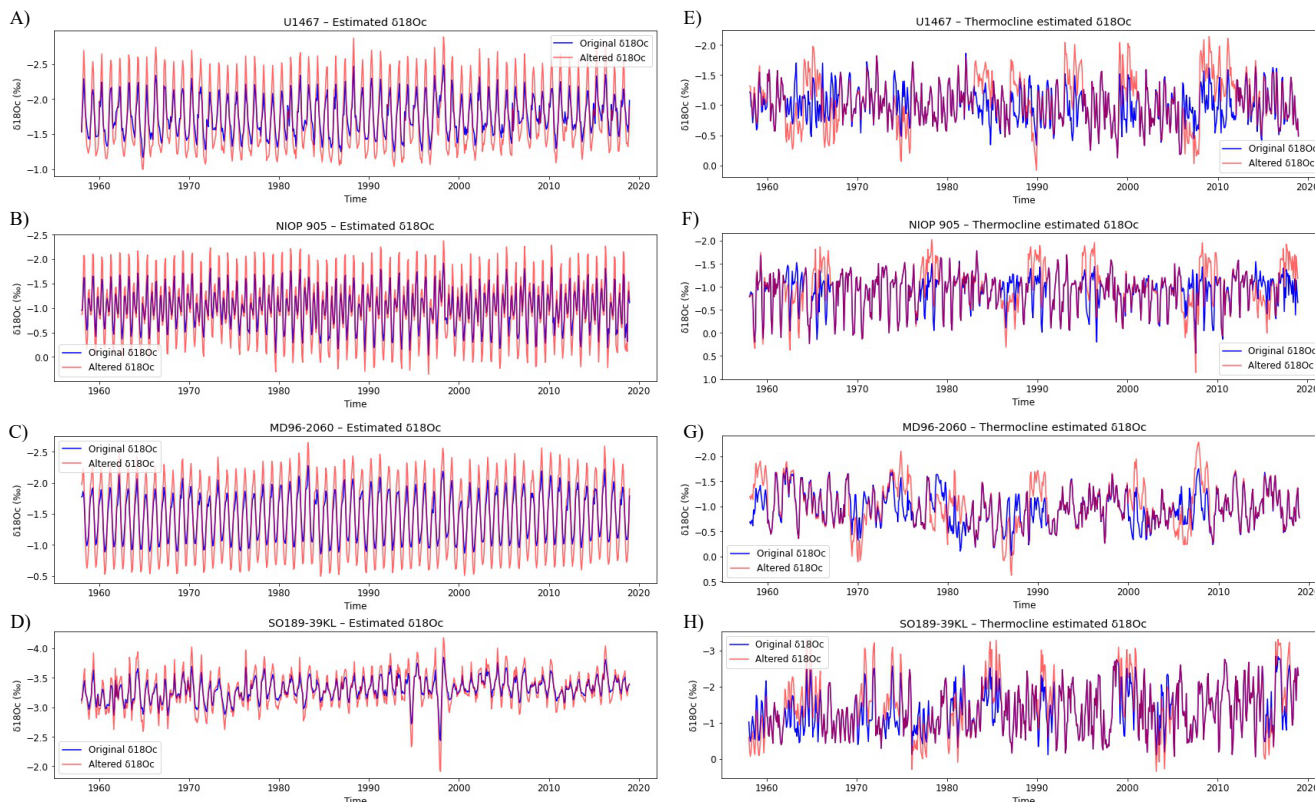
330 At the surface (Fig. 4A-D), we only change the seasonal variability by amplifying the annual oscillation of $\delta^{18}\text{O}_c$, which is
highly regular and characterized by a relatively high amplitude increase of 75% (sinusoidal pattern). The "Altered" scenario
(Fig 4A-B) clearly shows an amplification of seasonal extremes. Conversely, at the thermocline depth (Fig. 4E-H), the seasonal
signal remains unchanged and interannual anomalies appear, increasing/decreasing the total amplitude of variability. The
"Original" and "Altered" curves overlap in a more complex manner, highlighting interannual anomalies.

335 Distinct patterns emerge between the different oceanographic provinces. These time series form the basis of our statistical
distributions and provide a visual representation of how changes in the water-column structure directly affect the potential
isotopic signature recorded by individual shells.

340



345



350

355

360

Figure 4. Comparison of monthly reanalysis dataset for an “original” (blue curve) and “altered” (red curve) climate scenarios for the surface and thermocline. $\delta^{18}\text{O}_c$ calculated from monthly temperature and salinity from 1958 to 2018. A-D) Surface reanalysis dataset for Sites U1467, NIOP 905, and MD96-2060, SO189-39KL respectively. E-H) Thermocline reanalysis dataset for the same sites.

365

We turn then to the results of the IFA picking under the different scenarios to simulate synthetic IFA core-tops. Following what we said, we simulate an increase of seasonality for surface, that we will assimilate to *G. ruber* in our IFA analysis and an increase of the interannual variability for the thermocline that we associate with *N. dutertrei* for our IFA. Forward-modelled IFA $\delta^{18}\text{O}$ show an increase in the SD at each site for both depths in an altered climate (Fig. 5). A higher SD indicates a greater dispersion of values and increased variability in the simulated $\delta^{18}\text{O}$ -IFA values. At the surface, higher SD is observed at Sites NIOP 905 and MD96-2060, with 0.38 ‰ and 0.35 ‰ respectively for the original scenario, versus 0.69 ‰ and 0.61‰ respectively for the altered scenario. Site U1467 shows an increase in SD from 0.28 ‰ to 0.49 ‰, and Site SO189-39KL from 0.19 ‰ to 0.29 ‰. At thermocline depth, SD at Site SO189-39KL increases from 0.63 ‰ for the original dataset to 0.76 ‰ for the altered dataset. Site NIOP 905 shows an increase from 0.37 ‰ to 0.49 ‰, Site MD96-2060 from 0.34 ‰ to 0.46 ‰ and Site U1467 from 0.28 ‰ to 0.42 ‰.

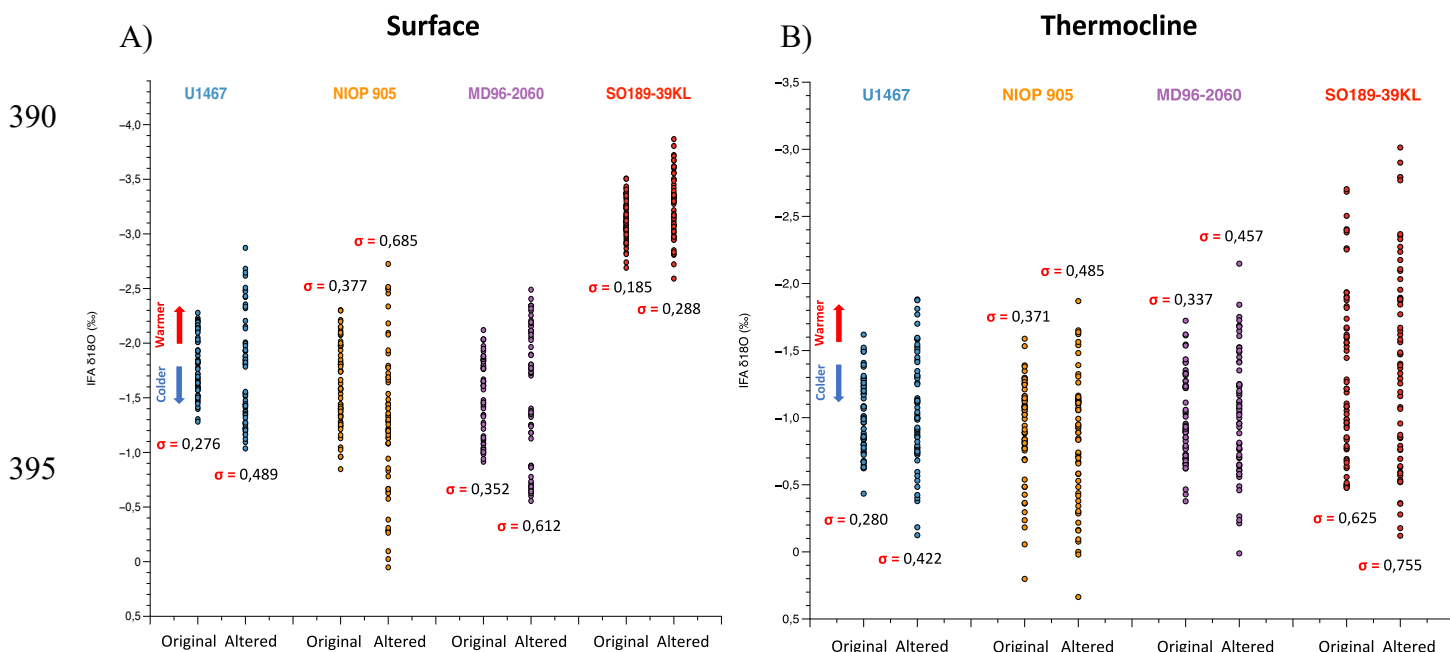
370

375



In summary, forward modelled IFA $\delta^{18}\text{O}$ values respond coherently with an increase in SD under altered scenario when seasonality or interannual variability is increased. Also, extreme IFA values become more frequent when overall variability increases, indicating that stronger interannual modes generate more anomalous conditions. We observe a significant difference between the western and eastern Indian Ocean for all scenarios with a higher surface variability for the western site and reduced variability for the eastern site, and the opposite tendency for thermocline variability with an increase for the east and a reduction for the west. Sites SO189-39KL and NIOP 905 seem to be the most sensitive to $\delta^{18}\text{O}$ changes at thermocline depth.

385



395

Figure 5. Modelled IFA $\delta^{18}\text{O}$ c (synthetic core top) values under original and altered climate variability scenarios at four sites in the Indian Ocean. Left panel: Surface modelled IFA variability associated with surface-dwelling *G. ruber*; right panel: Thermocline-depth modelled IFA variability associated with *N. dutertrei*. Two distributions are shown: the original modelled IFA $\delta^{18}\text{O}$ values (labelled "Original") and values obtained after artificially enhancing climate variability ("Altered"). The red and blue arrows highlight the relationship between $\delta^{18}\text{O}$ values and temperature (warmer = more negative values, colder = more positive values). SD for each distribution is reported for each dataset.

405

4.2 Core-top IFA analysis for sites MD96-2060 and U1467

We next turn to the core-top IFA analyses. For the surface, we use *G. ruber* and for the thermocline, *N. dutertrei*. The full dataset contains published and unpublished data. New data include an IFA dataset for the surface at Site MD96-2060 and three IFA datasets for the thermocline at Sites MD96-2060, U1467 and NIOP 905. $\delta^{18}\text{O}$ measurements on *G. ruber* IFA from Site MD96-2060 (n = 46) yield a mean value of -1.69‰ and a SD of 0.45‰ , including two outliers (Fig. 6). At the same site, new *N. dutertrei* IFA $\delta^{18}\text{O}$ values (n = 54) display a mean of -1.34‰ and a SD of 0.37‰ (Fig. 6C), with one outlier identified and removed prior to statistical analysis. Similarly, *N. dutertrei* measurements from Site U1467 (n = 44) have a mean value of -1.63‰ and a SD of 0.30‰ , with one outlier excluded from the dataset.

At Site NIOP 905, we use the *G. ruber* dataset published in Ganssen et al. (2011) along with unpublished *N. dutertrei* data measured on the same core-top (Gerald Ganssen, unpublished data). The *G. ruber* IFA isotopic values have a mean $\delta^{18}\text{O}$ of 1.53‰ and a SD of 0.56‰ , excluding 2 outliers. The *N. dutertrei* data (n = 38) are characterized by a mean $\delta^{18}\text{O}$ value of -0.02‰ and a SD of 0.53‰ (Fig. 6A). Finally, the SO189-39KL core reports a mean *G. ruber* IFA $\delta^{18}\text{O}$ of -2.93‰ , and a SD of 0.21‰ (Thirumalai et al., 2019). All dataset statistics are available in Fig. S2.

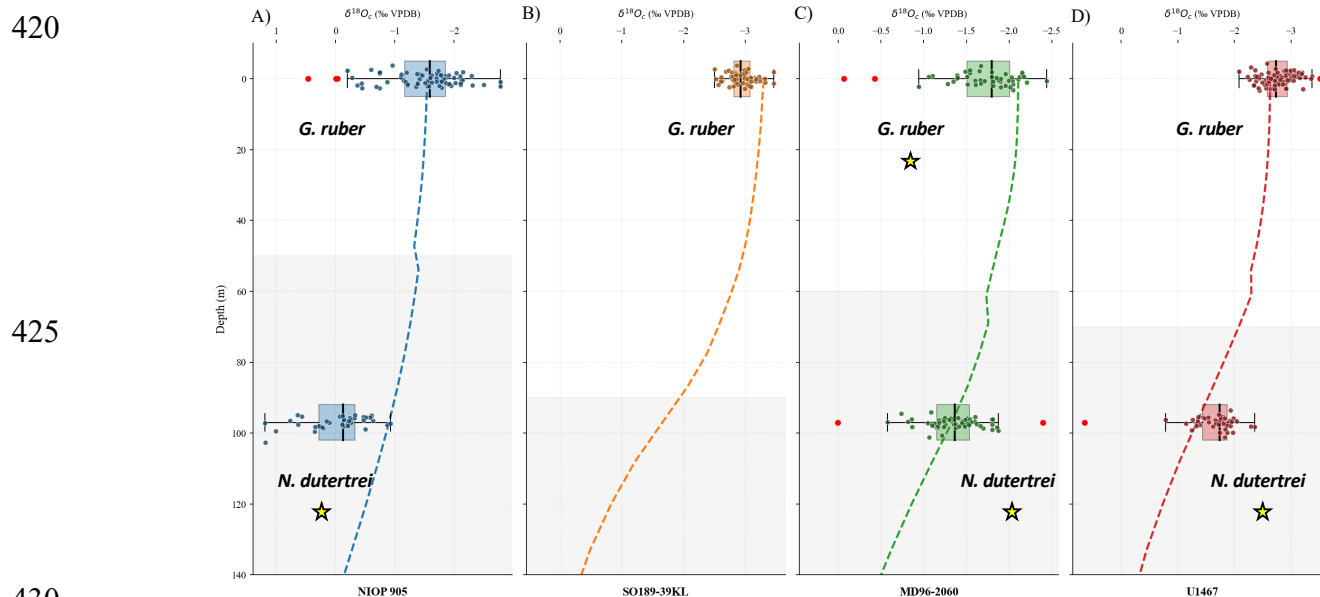


Figure 6. Vertical $\delta^{18}\text{O}_c$ profiles and IFA measured on core-tops across the Indian Ocean. The vertical $\delta^{18}\text{O}_c$ profiles (dashed lines) represent synthetic calcite values derived from modern instrumental reanalysis data, calculated using the Bemis et al., (1998) "high light" paleotemperature equation and regional $\delta^{18}\text{O}_w$ -salinity relationships, using the relationship presented in equations (1) and (2) for the surface and subsurface water depth, respectively. These hydrographic profiles are compared with Individual Foraminifera Analysis (Boxplots) results obtained from core-top sediments, representing the surface (0.5 m, *G. ruber*) and the thermocline (97 m, *N. dutertrei*). The gray shaded area represents the thermocline determined by a change in the temperature gradient. Yellow stars show new generated IFA dataset for this study.



5 Discussion

5.1 Interpretation of IFA- $\delta^{18}\text{O}_c$ datasets total variability signal

440 At the surface, the *G. ruber* IFA SD at sites MD96-2060 (0.34 ‰) and U1467 (0.28 ‰) are statistically similar (Fig. 6).
However, these values differ significantly from the SD observed at SO189-39KL (0.21 ‰) and NIOP 905 (0.56 ‰). SO189-
39KL is located in the warmest water and shows the lowest variability, whereas NIOP 905 is the coldest and has the highest
variability. The opposite pattern emerges when considering salinity, where the highest salinity is found at Site NIOP 905.
Thus, the most and least variable IFA datasets appear to reflect the regional extremes of temperature and salinity observed in
445 the ORAS5 reanalysis. Site NIOP 905 has a SD significantly higher than all the other sites (Fig. 6), indicating that this area is
somehow successfully capturing the expected total variability (Fig. 1c). This likely reflects the influence of a highly dynamic
seasonal system influenced by monsoonal winds (Schott and McReary., 2001) and its associated Ekman pumping during the
summer upwelling season, as originally suggested in Ganssen et al. (2011). The winter monsoon counterpart of this dynamical
upwelling system may also affect Site U1467, in the Maldives archipelago (Bassinot et al., 2011). However, Site U1467 is
450 supposed to be impacted in the same way as the equatorial MD96-2060 (Fig. 1), which is less influenced by seasonal wind-
induced upwelling and/or mixing. This suggests that, even though they show a similar SD the processes explaining their
variability are not the same and reflect regional influences. The permanent equatorial eastern Indian upwelling that produces
the lowest IFA variability (site SO189-39KL, SD of 0.21 ‰) may indicate that the modern thermocline depth is so deep (Fig.
6B) that, despite potential changes in upwelling activity, the surface IFA SD is very low at that site. The equatorial eastern
455 Indian Ocean off Sumatra is less influenced by monsoonal dynamics, as suggested by the stable and warm SST (Fig. 3). Here,
seasonal and interannual movements of the ITCZ in the Indonesian archipelago induce significant changes in the SSS (Fig. 3),
however these are not sufficient to significantly increase the IFA SD in this location (Fig. 4, 6).

At thermocline depth, IFA on *N. dutertrei* reveal a similar amplitude at Sites MD96-2060 and U1467 (SD of 0.30 ‰, Fig. 6B).
As in the surface, Site NIOP 905 records the highest subsurface SD (0.53 ‰). The pattern of variability at this site (Fig. 4B,
460 D) confirms that IFA results are mainly driven by seasonality even in subsurface. This suggests a deeply integrated response
to seasonal (monsoonal) forcing potentially suggesting a well-mixed water column from the surface to the thermocline depth.

We note that the most negative mean and the most reduced IFA results come from the warm, low-salinity Site SO189-39KL
(Fig. 1, 3), despite the equatorial upwelling that prevails year-round (Fig. 6). In contrast, the extremely highly dynamic
465 upwelling system offshore Somalia coincides with the core-top where the highest SD in IFA is reported (Fig. 6). Overall, these



deviations from the mean $\delta^{18}\text{O}_c$ profile as well as the differences in the SD at different sites imply that multiple dynamical and ecological processes are at play, and these need to be accounted for in the interpretation of planktonic foraminifera IFA.

5.2 Assessing proxy sensitivity through Forward-modelled IFA "Original" and "Altered" variability scenarios

470 To evaluate the sensitivity and spatial variability of IFA-derived $\delta^{18}\text{O}_c$ signals, we modelled four synthetic scenarios in which only salinity or temperature variability was either amplified or reduced. The original scenario aims to represent a synthetic core-top based on a random sampling of the reanalysis datasets presented in Fig. 4. The altered scenario is a sensitivity test that simulates a synthetic sample representing a time window when increased and decreased seasonality of interannual variability is imposed to the reanalysis dataset as shown in Fig. 5.

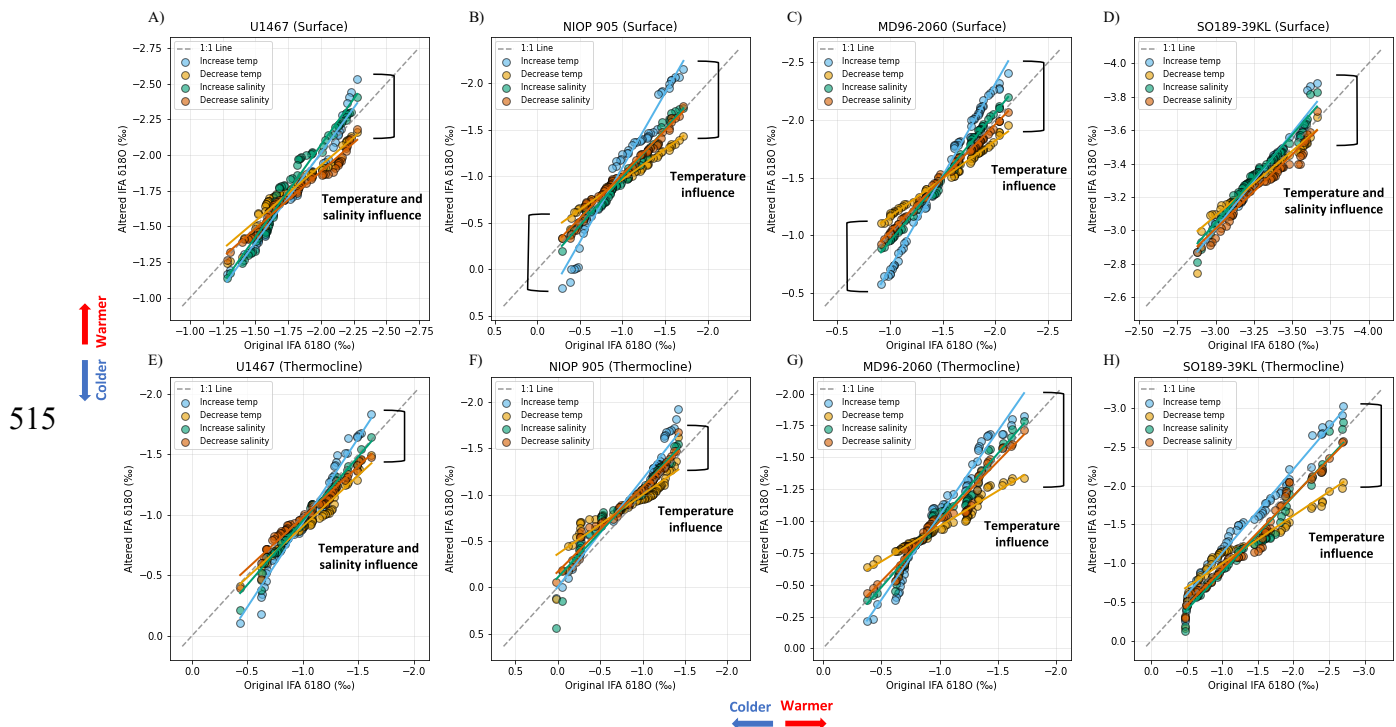
475 At the surface, the modelled results reveal a distinct spatial pattern of sensitivity to seasonal and interannual variability (Fig. 1). The south Indian coast, at site U1467, shows a coherent difference in the slopes between increased and reduced scenarios (Fig. 7A). Both changes in the SSS and SST annual cycle influence the IFA- $\delta^{18}\text{O}$, especially in the extreme high quantile of the distribution. This site, located in the path of the seasonally reversing West India Coastal Current (WICC) that transports fresher surface water from the Bay of Bengal to the Arabian Sea during winter and saline water from the Arabian Sea eastwards
480 during summer (Shankar et al., 2002), is sensitive to seasonal changes in SSS. The amplitude of SSS seasonality is set by the monsoonal system (Talley et al., 2011). Moreover, it also drives seasonal changes in temperature linked to upwelling dynamics during the southwest monsoon when Ekman pumping that advects waters upwelled from sites situated in the NIOP 905 region is stronger, reducing SST at Site U1467.

The Quantile-Quantile plot of Site NIOP 905, located offshore Somalia, south of the Arabian Sea, shows a dominant
485 temperature influence on IFA- $\delta^{18}\text{O}$ (Fig. 7B). The seasonal variation in SSS is less than 1 psu, whereas SST that reaches a maximum amplitude of 8.5°C (Fig. 3). This major temperature variability is associated with the strong seasonal upwelling during summer monsoon that leads to the shoaling of cold water-masses in this area (Vinayachandran et al., 2021). A second SST drop during the winter monsoon is also observed and is associated with wind-induced mixing (Fig. 3B), interspaced by periods of warm-water advection toward the NIOP 905 site. The IFA- $\delta^{18}\text{O}$ surface variability at Site MD96-2060 is also mainly
490 temperature-driven (Fig. 7C). The site is under the influence of a seasonally reversing surface current, the East African Coastal Current (Schott and McCreary, 2001; Schott et al., 2009), which is situated near the northern limit of the South Equatorial Current. Its boundary oscillates between 6°S and 9°S in response to the South Indian Ocean trade winds. At equatorial eastern Indian Ocean Site SO189-39KL, IFA- $\delta^{18}\text{O}$ shows both invariant temperature and salinity at seasonal timescales (Fig. 1). Not



only is the total IFA SD of the synthetic core-top IFA halved compared to other sites (Fig. 7D), but also an artificial increase
495 or decrease in its variability at the seasonal scale fails to clearly modify the slope of the Q-Q plots distributions.

Decomposition of the IFA- $\delta^{18}\text{O}$ signals at thermocline depth shows that they are mainly driven by temperature changes at all
sites (Fig. 7F-H), except for Site U1467, where salinity has a greater influence (Fig. 3, 7F). Although the seasonal temperature
cycle remains significant in the thermocline, the interannual variability manifests much more in the thermocline variability as
compared to that of surface waters (Fig. 3). Based on the climatological data, most of the IFA- $\delta^{18}\text{O}$ variations at interannual
500 scale are driven by temperature variability (Fig. 3). Given that salinity fluctuations remain minimal across all sites (less than
0.5 psu), we conclude that the influence of salinity on the interannual IFA- $\delta^{18}\text{O}$ signal is secondary, allowing thermocline-
dwelling species to be used primarily as a proxy for temperature-driven variability at these timescales. Site MD96-2060 appears
to be the most promising site for recording interannual variability with IFA at the thermocline depth. Many studies show that
this area is very sensitive to interannual event such as IOD, influencing upper water column temperature and sea surface
505 salinity (Yu et al., 2005; Qiu et al., 2012). Also, strong positive IOD events lead to significant seasonal upwelling, which
reduces SST. This is apparent in the Q-Q plots as a clear deviation in the slopes of the IFA distributions for site MD96-2060
(Fig. 7). Interestingly, the eastern equatorial Indian Ocean site SO189-39KL is also very sensitive to interannual variability
within the subsurface (Fig. 7). However, the surface seasonality is so muted in that core compared to other sites that any
changes in the altered IFA in the surface waters will be almost exclusively associated with changes in interannual variability
510 (Thirumalai et al., 2019).



515



520 **Figure 7.** Quantile–Quantile (QQ) plots comparing original and altered modelled IFA $\delta^{18}\text{O}$ distributions at four sites (U1467, NIOP 905,
MD96-2060 and SO189-39KL) for both surface (top row) and thermocline (bottom row) depths. Each panel shows the relationship between
the original modelled IFA $\delta^{18}\text{O}$ values (x-axis) and the altered distributions (y-axis), generated by applying synthetic perturbations to
temperature and salinity. Colored points represent different types of variability scenarios: temperature increase (red), temperature decrease
(blue), salinity increase (orange), and salinity decrease (green). The 1:1 line (dashed) indicates perfect agreement between original and
525 altered distributions.

Overall, our forward-modelling results through Q-Q plots demonstrate that IFA- $\delta^{18}\text{O}$ distributions coherently capture changes
in both seasonal and interannual climate variability across the Indian Ocean in surface- and subsurface-dwelling foraminifera,
respectively (Fig. 7). Specifically, surface-dwelling species such as *G. ruber* are excellent candidates to record monsoon-driven
530 seasonality, while thermocline-dwelling species will generally primarily reflect temperature-driven interannual anomalies
associated with IOD/ENSO dynamics. One exception to this is in regions where large freshwater inputs or mixing processes
occur, imprinting an important additional salinity influence (e.g., site U1467). This robust response at both depths validates
the use of IFA to identify the prevalence of extreme climatic events in the sedimentary record, even where salinity exerts a
secondary influence.

535 While these sensitivity experiments clarify how IFA signals theoretically respond to changing climate variability, the reliability
of our interpretations depends on the model's ability to replicate observed sedimentary data. In the following section, we
benchmark our forward-modelled results against the measured core-top distributions to assess the reproducibility of both
isotopic variance and mean signals.

540 **5.3 Benchmarking the forward model: Reproducibility of measured IFA- $\delta^{18}\text{O}$ variance and mean**

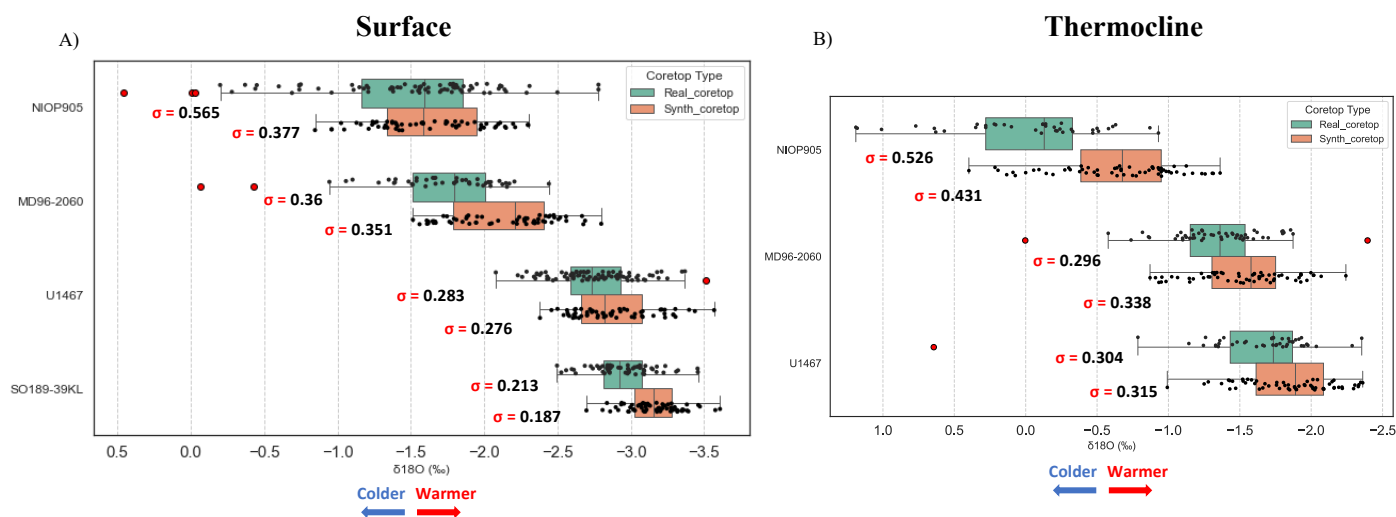
Previous studies have generated artificial IFA data in order to assess the ability of foraminifera to record Indian monsoon
variability (Thirumalai and Clemens., 2020), ENSO dynamics in the eastern equatorial Pacific (Thirumalai et al., 2013), or for
global IFA analysis with the Quantifa algorithm (Glaubke et al., 2021). Our study, which focuses on a streamlined script using
modern reanalysis datasets (ORAS5), provides a useful tool to simulate random foraminiferal picking that can effectively
545 reproduce the $\delta^{18}\text{O}$ distributions observed in measured Late Holocene core-top samples. We now compare our new IFA dataset
with Forward-modelled IFA using this new script as a tool to reproduce Late Holocene variability conditions for all sites.



At most sites, the forward-modelled (synthetic) and measured (real) core-top datasets show good agreement in their SD (Fig. 8), confirming that modern oceanographic variability is well captured by our simplified picking model. However, Site NIOP 905 is a notable exception, with real SD significantly higher than synthetic ones (0.56 ‰ vs. 0.38 ‰ for the surface and 0.53 ‰ vs. 0.43 ‰ for the thermocline). We also observe a systematic offset in absolute values across all sites: synthetic $\delta^{18}\text{O}$ distributions are consistently shifted towards more negative (warmer/fresher) values compared to the real core-top measurements. This offset, which can reach ~ 0.5 ‰ when comparing mean values, does not appear to affect the model's ability to simulate the range of climate variability and likely stems from factors such as foraminiferal vital effects, depth habitat uncertainties, or the older ages of the real Holocene core-top samples (which range from 0.1 to 3.8 kyr) relative to the synthetic modern ones.

555

560



565

Figure 8. Comparison between measured and modelled IFA $\delta^{18}\text{O}$ c distributions across multiple sites in the Indian Ocean for the surface (*G. ruber*-like) IFA (a) and the thermocline (*N. dutertrei*-like) IFA (b). For each site, panel shows the individual foraminiferal $\delta^{18}\text{O}$ distributions as boxplots (real data: in green; forward-modelled data: in orange). The Boxplots show the range between first and third quartiles (thin bars). Red dots from real_core-tops distribution are assimilated as outliers, defined with the 1,5 IQR method explained in section 3. The black line in each box represents the median value of each dataset.

570



5.3.1 Influence of anthropogenic warming and mean calcification depth on absolute offsets

575 These differences in mean $\delta^{18}\text{O}$ values could be linked to the fact that modelled IFA $\delta^{18}\text{O}$ values reflect conditions over the period 1958 to 2018 anthropogenic climate change influenced conditions. The Indian Ocean is the region that experienced the fastest warming (0.12°C per decade) over recent decades (Roxy et al., 2014).

580 The amplitude and frequency of extreme events such as ENSO, IOD and monsoon have already increased in the modern era due to anthropogenic global warming (Cai et al., 2013; 2014), and have been shown to intensify upwelling dynamics in regions such as the Arabian Sea and the Sumatra coast (Praveen et al., 2016; deCastro et al., 2015). As a result, simulations based on modern reanalysis datasets may yield higher $\delta^{18}\text{O}$ variability than what is recorded in Late Holocene core-tops. It may likely be slightly skewed towards warm anomalies, leading to an overestimation of natural baseline variability in the forward-modelling and may at least partly explain why synthetic core-top means are systematically lighter than core-top measurements (Fig. 8). Nevertheless, forward-modelling using ORAS5 reanalysis data produces similar SD values to core-tops where IFA- $\delta^{18}\text{O}$ was measured, except for the very dynamic NIOP 905 site.

585 Beyond the physical structure of the water column and historical warming trends, the biological complexities of the proxy, specifically the seasonal timing of shell production and the ecological preferences of each species, should be considered to explain the remaining differences in signal recording. Deviation from the synthetic core-top means could also represent a vital effect on the $\delta^{18}\text{O}$, which is traceable when planktonic foraminifera calcite $\delta^{18}\text{O}$ at equilibrium are compared (Fairbanks et al., 1982).

590

5.3.2 Impact of seasonality, shell flux, and ecology of planktonic foraminifera

One hypothesis about these offsets, could be linked to the complexity of simulating foraminiferal ecology (Scott et al., 2025), with uncertainties related to ecological niche and living depth of planktonic foraminifera that could explain the difference 595 between synthetic and real core-tops for Site NIOP 905. *G. ruber* is found in the Indian Ocean all year round and should represent mean annual conditions. On the other hand, simulation of foraminiferal growth shows that species such as *G. ruber* have a preferential maximum growth rate depending on the season and the region where they are found (Lombard et al., 2011). For the Somali margin, *G. ruber* shows a maximum vertical flux in March and to a lower extent in September during the inter-monsoon seasons (Figure S6 in Chaabane et al., 2023, Curry et al., 1992) contrasting with the other sites in this study where 600 maximum growth rates occur during boreal summer (August and September). In addition, the calcification depth of *G. ruber*, our target species, likely extends down to 50 m depth in the water column (Chaabane et al., 2026). In our modelling, we extracted data from a single depth from the reanalysis file (0.5 m) and not the mean of the estimated range of calcification depth, possibly leading to a shallow bias in our modelled IFA- $\delta^{18}\text{O}$. However, as this species remains in the mixed layer depth,



there should be limited changes between both estimates. Site NIOP 905 show minor changes in the mean values at different
605 depth for the surface mixed layer (Fig. S7).

N. dutertrei, our target thermocline species, is thought to grow mostly in September and October at site MD96-2060 and
U1467, in February for the eastern Indian Ocean and in August for NIOP 905 (Lombard et al., 2011). The peak in August
610 corresponds to the summer monsoon and the maximum intensity of the Somalian upwelling with strong advection of high-
nutrient waters (Schott and McCreary, 2001), while the second-order mixing events during the winter monsoon trigger a second
decrease in SST (Fig. 4). Interestingly, the thermocline $\delta^{18}\text{O}$ recorded in warmest and coldest months is of the same magnitude
as the ones recorded during extreme interannual events (Fig. 4), so it is difficult to attribute a shift in *N. dutertrei* IFA SD to a
change in seasonal vs. interannual shift in the thermocline variability regime. *N. dutertrei* is commonly found above the DCM
in tropical zones (Schmucker and Schiebel 2002), so this species is most often reported to adopt an opportunistic behavior
615 (Kroon and Ganssen 1989; Schiebel et al., 2004). Multiples studies show that the chlorophyll maximum off the Somalia coast
is found within the first 40 m from the surface (Lakshmi et al., 2020) during the peak of the summer upwelling when the
highest proportion of *N. dutertrei* may calcify and be directly influenced by temperature changes associated with cold water
advection, analogously to what has been recorded in the *G. bulloides* fluxes in sediment traps (Figure S6). Compared to *G.*
ruber, *N. dutertrei* could dwell over a large range of water depths (Chaabane et al 2026; Fairbanks et al., 1982). However, the
620 simulated thermocline SD is very close to the core-top IFA distribution (Fig. 8), except for NIOP 905. This highlights the fact
that studying the variability of *N. dutertrei* could help to reconstruct the potential impact of the summer monsoon and the
upwelling intensity at both seasonal and interannual scales. The extreme SD value associated with the real core-top of NIOP
905 (Fig. 7B) may represent extreme cold or warm thermocline temperatures (up to 1‰ warmer or colder than the mean),
suggesting that the SD of *N. dutertrei* is meaningful for tracking extreme events. Similar seasonal dynamics are observed in
625 the eastern Indian Ocean south of Java, where sediment traps also report that *N. dutertrei* and *G. bulloides* are more abundant
in boreal summer (August-September) when intense upwelling occurs (Mohtadi et al., 2009), as described for the Somalian
upwelling.

Overall, the IFA mean values of both species at all sites deviate from almost zero to values up to +/-1‰ when compared to the
630 calculated $\delta^{18}\text{O}_c$ profiles (Fig. 6). This likely indicates that the calcification depth or the seasonal variability of foraminiferal
fluxes differ from those expected under mean-annual surface and thermocline temperature and salinity conditions, thereby
could producing the observed deviations.

5.3.3 The role of the Salinity to $\delta^{18}\text{O}_w$ relationship

Additional uncertainties could be related to the choice of the salinity- $\delta^{18}\text{O}_w$ equation for each site to forward-model the
635 synthetic core-tops. For the subsurface water, we used an equation derived from the available dataset from Legrande and
Schmidt (2006) restricted to the tropical Indian Ocean (Fig. S8) that provides an average relationship of $\delta^{18}\text{O}_w = 0.26 \cdot S - 8.6$.



640 However, for the surface, multiple equations are used in studies focused on regional areas and these differ from the global Indian Ocean equation proposed by Legrande and Schmidt 2006 ($\delta^{18}\text{Ow} = 0.16 * \text{S} - 5.31$). For each study we used regional and derived equations adapted for each different area following Stainbank et al. (2021) for site U1467 ($\delta^{18}\text{Ow} = 0.28 * \text{S} - 9.24$), Thirumalai et al., (2019) for the eastern Indian Ocean ($\delta^{18}\text{Ow} = 0.16 * \text{S} - 5.31$), and ($\delta^{18}\text{Ow} = 0.26 * \text{S} - 8$) for the two other western Indian ocean sites, based on dataset extracted from Legrande and Schmidt (2006).

645 For NIOP 905 the few reported data of $\delta^{18}\text{Ow}$ and surface salinity presented in Ganssen et al., (2011) represent a relation of $\delta^{18}\text{Ow} = 0.12 * \text{S} - 4.03$, defining a very shallow slope. One possibility is that such seawater $\delta^{18}\text{O}$ and salinity measurements are representative of a limited area over a very short time window and do not reflect the mean oceanographic isotopic and salinity conditions in a regional, long-term context. Moreover, the nearest equation to this site established for the Arabian Sea by Delaygue et al., 2001 (i.e. $\delta^{18}\text{Ow} = 0.26 * \text{S} - 8.9$) indicates that the slope may be at least twice as large as that calculated using the in-situ data published in Ganssen et al. (2011). This discrepancy is particularly relevant in a region strongly affected by upwelling and mixing that may add a deeper component into the equation that may tend to make the slope even steeper than
650 in the surface. We note that the mean IFA- $\delta^{18}\text{Oc}$ generated is very sensitive of the $\delta^{18}\text{Osw} - \text{S}$ relationship in the forward model, and could be shifted to higher or lower $\delta^{18}\text{O}$ values with differences as large as 0.5 ‰ between two equations.

5.3.4 Impact of temporal integration, sedimentation rates, and core-top age

655 Another source of uncertainty resides in using a framework of cores that have different sedimentation rates. Our synthetic IFA distributions are generated from a 60-year instrumental window (1958–2018), but our core-top samples represent a time-averaged signal determined by the local sedimentation rate and the amount of time averaged within the 1-cm wide samples after it has been homogenized by bioturbation. Based on regional sedimentation rates, the temporal window integrated into each 1-cm sample varies significantly across the basin. For sites SO189-39KL, NIOP 905, and U1467, sediment rates are very
660 high and range from 20 to 40 cm/kyr, which represent approximately 25 to 50 years for this thickness (Mohtadi et al., 2014; Ivanochko et al., 2005; Stainbank et al., 2020). Site MD96-2060 has a much lower sedimentation rate (6–8 cm/kyr), so that a 1-cm sample may integrate 125 to 166 years without considering potential bioturbation effects. A scenario in which the bioturbated layer would reach 10 cm thickness would suggest that the MD96-2060 core-top integrates oceanic conditions over the last millennium. This may lead to an overestimation of the total variability simulated in our core-top because foraminifera
665 potentially lived under conditions when the climate background was different. However, a higher SD in the real vs synthetic core-top is not seen in our data. Our core-top age at site MD96-2060 is ~3.8 kyr, which is much older than the core-tops at other sites (Table 1), indicating that the IFA here recorded environmental conditions during the late Holocene, not the last few centuries. Observing the results from real and synthetic core-tops (Fig. 8) shows that even with a different sedimentation rate



and core-top age, site MD96-2060 exhibits the same variability with the same SD as most of the other sites except for NIOP
670 905. The range of seasonal and interannual climate, hence likely, remained relatively stable between the modern and Late
Holocene periods.

Overall, the comparison of SD between forward-modelled and core-top IFA reveals good agreement, though a systematic
offset in mean values is observed across all sites. This offset likely reflects a potential combination of anthropogenic warming
675 trends embedded in the ORAS5 reanalysis and uncertainties in the regional $\delta^{18}\text{Ow-S}$ relationship, both of which would shift
synthetic distributions toward lighter values. At site NIOP 905, the higher SD in real core-tops point to additional factors,
related to the strong upwelling dynamics of the Somali margin. However, the most probable primary source of discrepancy in
both mean values and SD across all sites lies in the seasonal variability of foraminiferal fluxes and ecological factors, as
discussed in section 5.3.2. Temporal integration of the IFA signal and sedimentation rate may introduce additional uncertainties
680 but are expected to have a comparatively minor influence on the observed offsets.

6. Summary & Conclusion

685 We evaluated the sensitivity and spatial variability of individual foraminifera $\delta^{18}\text{Oc}$ signals across the Indian Ocean by
combining forward-modelled synthetic core-tops with real core-top measurements. Our approach shows that forward-
modelling synthetic IFA with modern reanalysis data can reproduce the SD of $\delta^{18}\text{Oc}$ observed in Late Holocene core-tops,
providing a robust framework to simulate natural variability. The simulated SD are in good agreement with those derived from
real IFA data for both surface and thermocline-dwelling species.

690 Forward-modelled IFA enables statistical analyses and spatial comparisons of modern variability across the Indian Ocean, as
well as testing the effects of altered climate variability scenarios. When statistically modified, the seasonality or interannual
variability changed $\delta^{18}\text{Oc}$ show coherent response to higher amplitude showing that this method provides a tool to record this
type of high frequency variability. Amplification or reduction of seasonal and interannual variability highlights the ability of
695 IFA $\delta^{18}\text{Oc}$ to record extreme events.

Our results indicate that at the surface, $\delta^{18}\text{Oc}$ variability from western and northern Indian Ocean (MD96-2060, NIOP 905,
and U1467) shows strong sensitivity to seasonal variability associated with monsoon dynamics and upwelling processes,
whereas the equatorial eastern site (SO189-39KL) is less affected by seasonality and more influenced by interannual events
700 associated to phenomena such as IOD and ENSO influencing the temperature variability. At thermocline depth, $\delta^{18}\text{Oc}$
variability is largely driven by temperature changes, with salinity exerting a secondary influence except in regions affected by
strong freshwater inputs or mixing such as site U1467. Overall, the good agreement between forward-modelled and measured



705 IFA distributions demonstrates that the modern climate variability captured by IFA depends primarily on the depth habitat of the target species and the regional oceanographic setting. In the western Indian Ocean, surface-dwelling *G. ruber* predominantly records monsoon-driven seasonal variability, while thermocline-dwelling *N. dutertrei* appears more sensitive to interannual forcing, likely reflecting IOD-driven temperature anomalies at thermocline depth. Site NIOP 905 stands as a notable exception, where the shallow thermocline and intense seasonal upwelling dynamics impart a strong seasonal imprint on the *N. dutertrei* and lead to a mix signal of the total variability.

710 Several sources of uncertainty remain, especially at site NIOP 905 that highlights a significant difference in SD between real and synthetic core-top. These differences may arise from ecological factors, including the actual depth range and seasonal growth patterns of foraminiferal species and their opportunistic behaviour, as well as from the choice of salinity– $\delta^{18}\text{O}$ equations used for forward-modelling. Also, biases in reanalysis products, especially near coastal regions, may influence the mean $\delta^{18}\text{O}$ signal, though their effect on variability metrics appears limited and unclear.

715 The method introduces a template for interpreting IFA- $\delta^{18}\text{O}$ and its associated spatial fingerprints under different climate backgrounds, to be applied to downcore measurements. Our results allow for a clear distinction between regions dominated by seasonal forcings such as in monsoon systems and upwelling regions, as well as those governed by interannual climate modes. This framework establishes a robust starting point for future studies aiming to reconstruct past seasonal and interannual climate variability using individual foraminifera analysis $\delta^{18}\text{O}$.

Code and data availability

725 The Python code used to generate the forward-modelled $\delta^{18}\text{O}$ datasets is openly available on GitHub at https://github.com/yoyolich/Lichterfeld2026-IFA-forward-model_2026. The new individual foraminifera analysis dataset presented in this study is available in the open access SEANOE data repository at <https://doi.org/10.17882/113513>. Previously published individual foraminifera analysis datasets used for comparison are available in the studies cited in the references.

Author contributions

730 YL, GL, and CTB conceptualized the study. Formal analysis was carried out by YL, and $\delta^{18}\text{O}$ measurements and validation were carried out by CS and LV. CTB and GL were responsible for funding acquisition and project supervision. The methodology was designed by YL, GL and KT. YL performed all coding and data visualisation, and wrote the initial draft of the manuscript. CTB, GL, KT, TDG, and LV reviewed and edited the manuscript draft.



Competing interests

735

The authors declare that they have no conflict of interest.

Acknowledgements

740

We thank Stephanie Stainbank, Elias Samankassou, and Torin Cannings for sharing sample material from IODP Site U1467 and enabling us to perform IFA analyses. We thank Gerald Ganssen for providing useful unpublished data from Site NIOP 905 for use in this paper. We thank Sonia Chaabane for useful discussions on the FORCIS database and foraminiferal ecology.

Financial support

This research was funded by a PhD studentship from the French Ministry of Research and Higher Education awarded to YL, and by the French ANR project ITCH (ANR-22-EDIR-0003-01), awarded to CTB.

References

745

Abram, N. J., Gagan, M. K., Cole, J. E., Hantoro, W. S., and Mudelsee, M.: Recent intensification of tropical climate variability in the Indian Ocean, *Nature Geoscience*, 1, 849–853, 2008.

Aldrian, E. and Susanto, R. D.: Identification of three dominant rainfall regions within Indonesia and their relationship to sea surface temperature, *International Journal of Climatology*, 23, 1435–1452, 2003.

750

Anderson, W. B., Seager, R., Baethgen, W., Cane, M., and You, L.: Synchronous crop failures and climate-forced production variability, *Sci. Adv.*, 5, eaaw1976, <https://doi.org/10.1126/sciadv.aaw1976>, 2019.

Bassinot, F. C., Marzin, C., Braconnot, P., Marti, O., Mathien-Blard, E., Lombard, F., and Bopp, L.: Holocene evolution of summer winds and marine productivity in the tropical Indian Ocean in response to insolation forcing: data-model comparison, *Climate of the Past*, 7, 815–829, <https://doi.org/10.5194/cp-7-815-2011>, 2011.

755

Behara, A. and Vinayachandran, P. N.: An OGCM study of the impact of rain and river water forcing on the Bay of Bengal, *Journal of Geophysical Research: Oceans*, 121, 2425–2446, <https://doi.org/10.1002/2015JC011325>, 2016.

Bemis, B. E., Spero, H. J., Bijma, J., and Lea, D. W.: Reevaluation of the oxygen isotopic composition of planktonic foraminifera: Experimental results and revised paleotemperature equations, *Paleoceanography*, 13, 150–160, 1998.

Benway, H. M. and Mix, A. C.: Oxygen isotopes, upper-ocean salinity, and precipitation sources in the eastern tropical Pacific, *Earth and Planetary Science Letters*, 224, 493–507, <https://doi.org/10.1016/j.epsl.2004.05.014>, 2004.



- 760 Bienzobas Montávez, N., Thirumalai, K., and Marino, G.: Shell Reworking Impacts on Climate Variability Reconstructions Using Individual Foraminiferal Analyses, *Paleoceanog and Paleoclimatol*, 39, e2023PA004663, <https://doi.org/10.1029/2023PA004663>, 2024.
- Bouvier-Soumagnac, Y. and Duplessy, J.-C.: Carbon and oxygen isotopic composition of planktonic foraminifera from laboratory culture, plankton tows and Recent sediment; implications for the reconstruction of paleoclimatic conditions and of the global carbon cycle, *The Journal of Foraminiferal Research*, 15, 302–320, <https://doi.org/10.2113/gsjfr.15.4.302>, 1985.
- 765 Cai, W., Zheng, X.-T., Weller, E., Collins, M., Cowan, T., Lengaigne, M., Yu, W., and Yamagata, T.: Projected response of the Indian Ocean Dipole to greenhouse warming, *Nature Geosci*, 6, 999–1007, <https://doi.org/10.1038/ngeo2009>, 2013.
- Cai, W., Borlace, S., Lengaigne, M., van Rensch, P., Collins, M., Vecchi, G., Timmermann, A., Santoso, A., McPhaden, M. J., Wu, L., England, M. H., Wang, G., Guilyardi, E., and Jin, F.-F.: Increasing frequency of extreme El Niño events due to greenhouse warming, *Nature Clim Change*, 4, 111–116, <https://doi.org/10.1038/nclimate2100>, 2014.
- 770 Chaabane, S., de Garidel-Thoron, T., Giraud, X., Schiebel, R., Beaugrand, G., Brummer, G.-J., Casajus, N., Greco, M., Grigoratou, M., Howa, H., Jonkers, L., Kucera, M., Kuroyanagi, A., Meilland, J., Monteiro, F., Mortyn, G., Almogi-Labin, A., Asahi, H., Avnaim-Katav, S., Bassinot, F., Davis, C. V., Field, D. B., Hernández-Almeida, I., Herut, B., Hosie, G., Howard, W., Jentzen, A., Johns, D. G., Keigwin, L., Kitchener, J., Kohfeld, K. E., Lessa, D. V. O., Manno, C., Marchant, M., Ofstad, S., Ortiz, J. D., Post, A., Rigual-Hernandez, A., Rillo, M. C., Robinson, K., Sagawa, T., Sierro, F., Takahashi, K. T., Torfstein, A., Venancio, I., Yamasaki, M., and Ziveri, P.: The FORCIS database: A global census of planktonic Foraminifera from ocean waters, *Sci Data*, 10, 354, <https://doi.org/10.1038/s41597-023-02264-2>, 2023.
- 775 Chaabane, S., Schiebel, R., Meilland, J., Brummer, G.-J. A., Mortyn, P. G., Sulpis, O., Chalk, T. B., Giraud, X., Howa, H., Kuroyanagi, A., Beaugrand, G., and Garidel-Thoron, T. D.: Reassessment of the global distribution and diversity of modern planktonic Foraminifera from the FORCIS database, <https://doi.org/10.22541/au.173991286.60773031/v1>, 18 February 2025.
- 780 Curry, W. B., Ostermann, D., Guptha, M. V. s., and Ittekkot, V.: Foraminiferal production and monsoonal upwelling in the Arabian Sea: Evidence from sediment traps, *Geol. Soc. London Spec. Publ.*, 64, <https://doi.org/10.1144/GSL.SP.1992.064.01.06>, 1992.
- Dauvier, J., Beaufort, L., Sonzogni, C., Bolton, C., Mazur, J. C., Kazuyo, T., Rapuc, W., Thouveny, N., Lichterfeld, Y., and Vidal, L.: Isotopic Imprints of Coccolithophore Blooms Overthe Past Million Years, *Copernicus Meetings*, 2026.
- 785 Delaygue, G., Bard, E., Rollion, C., Jouzel, J., Stiévenard, M., Duplessy, J., and Ganssen, G.: Oxygen isotope/salinity relationship in the northern Indian Ocean, *J. Geophys. Res.*, 106, 4565–4574, <https://doi.org/10.1029/1999JC000061>, 2001.
- Fairbanks, R. G., Sverdløve, M., Free, R., Wiebe, P. H., and Bé, A. W.: Vertical distribution and isotopic fractionation of living planktonic foraminifera from the Panama Basin, *Nature*, 298, 841–844, 1982.
- 790 Feely, R. A., Sabine, C. L., Lee, K., Berelson, W., Kleypas, J., Fabry, V. J., and Millero, F. J.: Impact of anthropogenic CO₂ on the CaCO₃ system in the oceans, *Science*, 305, 362–366, <https://doi.org/10.1126/science.1097329>, 2004.



- Fehrenbacher, J. S., Hupp, B. N., Branson, O., Evans, D., Foster, G. L., Glock, N., Thirumalai, K., and Wycech, J.: INDIVIDUAL FORAMINIFERAL ANALYSES: A REVIEW OF CURRENT AND EMERGING GEOCHEMICAL TECHNIQUES, *Journal of Foraminiferal Research*, 54, 312–331, <https://doi.org/10.61551/gsjfr.54.4.312>, 2024.
- 795 Ford, H. L., Ravelo, A. C., and Polissar, P. J.: Reduced El Niño–Southern Oscillation during the last glacial maximum, *Science*, 347, 255–258, 2015.
- Fousiya, T. S., Parekh, A., and Gnanaseelan, C.: Interannual variability of upper ocean stratification in Bay of Bengal: observational and modeling aspects, *Theor Appl Climatol*, 126, 285–301, <https://doi.org/10.1007/s00704-015-1574-z>, 2016.
- Gadgil, S.: The Indian Monsoon and Its Variability, *Annual Review of Earth and Planetary Sciences*, 31, 429–467, 800 <https://doi.org/10.1146/annurev.earth.31.100901.141251>, 2003.
- Ganssen, G. M., Peeters, F. J. C., Metcalfe, B., Anand, P., Jung, S. J. A., Kroon, D., and Brummer, G.-J. A.: Quantifying sea surface temperature ranges of the Arabian Sea for the past 20 000 years, *Climate of the Past*, 7, 1337–1349, <https://doi.org/10.5194/cp-7-1337-2011>, 2011.
- Glaubke, R. H., Thirumalai, K., Schmidt, M. W., and Hertzberg, J. E.: Discerning Changes in High-Frequency Climate 805 Variability Using Geochemical Populations of Individual Foraminifera, *Paleoceanography and Paleoclimatology*, 36, e2020PA004065, <https://doi.org/10.1029/2020PA004065>, 2021.
- Hood, R. R., Beckley, L. E., and Wiggert, J. D.: Biogeochemical and ecological impacts of boundary currents in the Indian Ocean, *Progress in Oceanography*, 156, 290–325, <https://doi.org/10.1016/j.pocean.2017.04.011>, 2017.
- Ivanochko, T. S., Ganeshram, R. S., Brummer, G.-J. A., Ganssen, G., Jung, S. J. A., Moreton, S. G., and Kroon, D.: Variations 810 in tropical convection as an amplifier of global climate change at the millennial scale, *Earth and Planetary Science Letters*, 235, 302–314, <https://doi.org/10.1016/j.epsl.2005.04.002>, 2005.
- Izumo, T., Montégut, C. B., Luo, J.-J., Behera, S. K., Masson, S., and Yamagata, T.: The Role of the Western Arabian Sea Upwelling in Indian Monsoon Rainfall Variability, *Journal of Climate*, 21, 5603–5623, <https://doi.org/10.1175/2008JCLI2158.1>, 2008.
- 815 Kemle-von Mücke, S. and Oberhänsli, H.: The Distribution of Living Planktic Foraminifera in Relation to Southeast Atlantic Oceanography, in: *Use of Proxies in Paleoceanography: Examples from the South Atlantic*, edited by: Fischer, G. and Wefer, G., Springer, Berlin, Heidelberg, 91–115, https://doi.org/10.1007/978-3-642-58646-0_3, 1999.
- Kroon, D. and Ganssen, G.: Northern Indian Ocean upwelling cells and the stable isotope composition of living planktonic foraminifers, *Deep Sea Research Part A. Oceanographic Research Papers*, 36, 1219–1236, [https://doi.org/10.1016/0198-0149\(89\)90102-7](https://doi.org/10.1016/0198-0149(89)90102-7), 1989.
- 820 Lakshmi, R. S., Chatterjee, A., Prakash, S., and Mathew, T.: Biophysical Interactions in Driving the Summer Monsoon Chlorophyll Bloom Off the Somalia Coast, *Journal of Geophysical Research: Oceans*, 125, e2019JC015549, <https://doi.org/10.1029/2019JC015549>, 2020.
- Leduc, G., Vidal, L., Cartapanis, O., and Bard, E.: Modes of eastern equatorial Pacific thermocline variability: Implications 825 for ENSO dynamics over the last glacial period, *Paleoceanography*, 24, <https://doi.org/10.1029/2008PA001701>, 2009.



- LeGrande, A. N. and Schmidt, G. A.: Global gridded data set of the oxygen isotopic composition in seawater, *Geophysical Research Letters*, 33, <https://doi.org/10.1029/2006GL026011>, 2006.
- Lombard, F., Labeyrie, L., Michel, E., Bopp, L., Cortijo, E., Retailliau, S., Howa, H., and Jorissen, F.: Modelling planktic foraminifer growth and distribution using an ecophysiological multi-species approach, *Biogeosciences*, 8, 853–873, <https://doi.org/10.5194/bg-8-853-2011>, 2011.
- 830 Mayorga-Adame, C. G., Batchelder, H. P., and Spitz, Y. H.: Modeling larval connectivity of coral reef organisms in the Kenya-Tanzania region, *Frontiers in Marine Science*, 4, 92, 2017.
- Mohtadi, M., Steinke, S., Groeneveld, J., Fink, H. G., Rixen, T., Hebbeln, D., Donner, B., and Herunadi, B.: Low-latitude control on seasonal and interannual changes in planktonic foraminiferal flux and shell geochemistry off south Java: A sediment trap study, *Paleoceanography*, 24, <https://doi.org/10.1029/2008PA001636>, 2009.
- 835 Mohtadi, M., Lückge, A., Steinke, S., Groeneveld, J., Hebbeln, D., and Westphal, N.: Late Pleistocene surface and thermocline conditions of the eastern tropical Indian Ocean, *Quaternary Science Reviews*, 29, 887–896, <https://doi.org/10.1016/j.quascirev.2009.12.006>, 2010.
- Mohtadi, M., Oppo, D. W., Lückge, A., DePol-Holz, R., Steinke, S., Groeneveld, J., Hemme, N., and Hebbeln, D.:
840 Reconstructing the thermal structure of the upper ocean: Insights from planktic foraminifera shell chemistry and alkenones in modern sediments of the tropical eastern Indian Ocean, *Paleoceanography*, 26, <https://doi.org/10.1029/2011PA002132>, 2011.
- Mohtadi, M., Prange, M., Oppo, D. W., De Pol-Holz, R., Merkel, U., Zhang, X., Steinke, S., and Lückge, A.: North Atlantic forcing of tropical Indian Ocean climate, *Nature*, 509, 76–80, <https://doi.org/10.1038/nature13196>, 2014.
- Park, I.-H., Yeh, S.-W., Min, S.-K., Ham, Y.-G., and Kirtman, B. P.: Present-day warm pool constrains future tropical
845 precipitation, *Commun Earth Environ*, 3, 310, <https://doi.org/10.1038/s43247-022-00620-5>, 2022.
- Peterson, L. C. and Prell, W. L.: Carbonate dissolution in Recent sediments of the eastern equatorial Indian Ocean: Preservation patterns and carbonate loss above the lysocline, *Marine Geology*, 64, 259–290, [https://doi.org/10.1016/0025-3227\(85\)90108-2](https://doi.org/10.1016/0025-3227(85)90108-2), 1985.
- Praveen, V., Ajayamohan, R. S., Valsala, V., and Sandeep, S.: Intensification of upwelling along Oman coast in a warming
850 scenario, *Geophysical Research Letters*, 43, 7581–7589, <https://doi.org/10.1002/2016GL069638>, 2016.
- Qiu, Y., Cai, W., Li, L., and Guo, X.: Argo profiles variability of barrier layer in the tropical Indian Ocean and its relationship with the Indian Ocean Dipole, *Geophysical Research Letters*, 39, <https://doi.org/10.1029/2012GL051441>, 2012.
- Rasmusson, E. M. and Carpenter, T. H.: Variations in Tropical Sea Surface Temperature and Surface Wind Fields Associated with the Southern Oscillation/El Niño, *Monthly Weather Review*, 110, 354–384, [https://doi.org/10.1175/1520-0493\(1982\)110<0354:VITSST>2.0.CO;2](https://doi.org/10.1175/1520-0493(1982)110<0354:VITSST>2.0.CO;2), 1982.
- 855 Roxy, M. K., Ritika, K., Terray, P., and Masson, S.: The Curious Case of Indian Ocean Warming, *Journal of Climate*, 27, 8501–8509, <https://doi.org/10.1175/JCLI-D-14-00471.1>, 2014.
- Saji, N. H., Goswami, B. N., Vinayachandran, P. N., and Yamagata, T.: A dipole mode in the tropical Indian Ocean, *Nature*, 401, 360–363, <https://doi.org/10.1038/43854>, 1999.



- 860 Sankar, S., Vijaykumar, P., Abhilash, S., and Mohanakumar, K.: Influence of the strongest positive Indian Ocean Dipole and an El Niño Modoki event on the 2019 Indian summer monsoon, *Dynamics of Atmospheres and Oceans*, 95, 101235, <https://doi.org/10.1016/j.dynatmoce.2021.101235>, 2021.
- Schiebel, R., Zeltner, A., Treppke, U. F., Waniek, J. J., Bollmann, J., Rixen, T., and Hemleben, C.: Distribution of diatoms, coccolithophores and planktic foraminifers along a trophic gradient during SW monsoon in the Arabian Sea, *Marine Micropaleontology*, 51, 345–371, <https://doi.org/10.1016/j.marmicro.2004.02.001>, 2004.
- 865 Schmidt, G. A., LeGrande, A. N., and Hoffmann, G.: Water isotope expressions of intrinsic and forced variability in a coupled ocean-atmosphere model, *Journal of Geophysical Research: Atmospheres*, 112, <https://doi.org/10.1029/2006JD007781>, 2007.
- Schmuker, B. and Schiebel, R.: Planktic foraminifers and hydrography of the eastern and northern Caribbean Sea, *Marine Micropaleontology*, 46, 387–403, [https://doi.org/10.1016/S0377-8398\(02\)00082-8](https://doi.org/10.1016/S0377-8398(02)00082-8), 2002.
- 870 Schott, F. A. and McCreary, J. P.: The monsoon circulation of the Indian Ocean, *Progress in Oceanography*, 51, 1–123, [https://doi.org/10.1016/S0079-6611\(01\)00083-0](https://doi.org/10.1016/S0079-6611(01)00083-0), 2001.
- Schott, F. A., Xie, S.-P., and McCreary Jr., J. P.: Indian Ocean circulation and climate variability, *Reviews of Geophysics*, 47, <https://doi.org/10.1029/2007RG000245>, 2009.
- Scott, J., Coenen, D., and Jung, S.: Millennial-scale sea surface temperatures of the western Arabian Sea between 37–
875 67 ka BP, *Climate of the Past*, 21, 1343–1357, <https://doi.org/10.5194/cp-21-1343-2025>, 2025.
- Shankar, D., Vinayachandran, P. N., and Unnikrishnan, A. S.: The monsoon currents in the north Indian Ocean, *Progress in Oceanography*, 52, 63–120, [https://doi.org/10.1016/S0079-6611\(02\)00024-1](https://doi.org/10.1016/S0079-6611(02)00024-1), 2002.
- Singh, A., Jani, R. A., and Ramesh, R.: Spatiotemporal variations of the $\delta^{18}\text{O}$ –salinity relation in the northern Indian Ocean, *Deep Sea Research Part I: Oceanographic Research Papers*, 57, 1422–1431, <https://doi.org/10.1016/j.dsr.2010.08.002>, 2010.
- 880 Stainbank, S., Kroon, D., Rüggeberg, A., Raddatz, J., Leau, E. S. de, Zhang, M., and Spezzaferri, S.: Controls on planktonic foraminifera apparent calcification depths for the northern equatorial Indian Ocean, *PLOS ONE*, 14, e0222299, <https://doi.org/10.1371/journal.pone.0222299>, 2019.
- Stainbank, S., Spezzaferri, S., De Boever, E., Bouvier, A.-S., Chilcott, C., de Leau, E. S., Foubert, A., Kunkelova, T., Pichevin, L., Raddatz, J., Rüggeberg, A., Wright, J. D., Yu, S. M., Zhang, M., and Kroon, D.: Assessing the impact of diagenesis on
885 foraminiferal geochemistry from a low latitude, shallow-water drift deposit, *Earth and Planetary Science Letters*, 545, 116390, <https://doi.org/10.1016/j.epsl.2020.116390>, 2020.
- Stainbank, S., Kroon, D., de Leau, E. S., and Spezzaferri, S.: Using past interglacial temperature maxima to explore transgressions in modern Maldivian coral and *Amphistegina* bleaching thresholds, *Sci Rep*, 11, 10267, <https://doi.org/10.1038/s41598-021-89697-0>, 2021.
- 890 Susanto, R. D., Gordon, A. L., and Zheng, Q.: Upwelling along the coasts of Java and Sumatra and its relation to ENSO, *Geophysical Research Letters*, 28, 1599–1602, <https://doi.org/10.1029/2000GL011844>, 2001.



- Swain, D. L., Prein, A. F., Abatzoglou, J. T., Albano, C. M., Brunner, M., Diffenbaugh, N. S., Singh, D., Skinner, C. B., and Touma, D.: Hydroclimate volatility on a warming Earth, *Nat Rev Earth Environ*, 6, 35–50, <https://doi.org/10.1038/s43017-024-00624-z>, 2025.
- 895 Talley, L., Pickard, G. L., Emery, W., and Swift, J. H.: *Descriptive physical oceanography: An introduction: Sixth edition*, *Descriptive Physical Oceanography: An Introduction: Sixth Edition*, 1–555, 2011.
- Thirumalai, K. and Clemens, S. C.: Monsoon Reconstructions using Bulk and Individual Foraminiferal Analyses in Marine Sediments Offshore India, *Current Science*, 119, 328, <https://doi.org/10.18520/cs/v119/i2/328-334>, 2020.
- Thirumalai, K., Partin, J. W., Jackson, C. S., and Quinn, T. M.: Statistical constraints on El Niño Southern Oscillation reconstructions using individual foraminifera: A sensitivity analysis, *Paleoceanography*, 28, 401–412, <https://doi.org/10.1002/palo.20037>, 2013.
- 900 Thirumalai, K., DiNezio, P. N., Tierney, J. E., Puy, M., and Mohtadi, M.: An El Niño Mode in the Glacial Indian Ocean?, *Paleoceanog and Paleoclimatol*, 34, 1316–1327, <https://doi.org/10.1029/2019PA003669>, 2019.
- Thirumalai, K., DiNezio, P. N., Partin, J. W., Liu, D., Costa, K., and Jacobel, A.: Future increase in extreme El Niño supported by past glacial changes, *Nature*, 634, 374–380, <https://doi.org/10.1038/s41586-024-07984-y>, 2024.
- 905 Thirumalai, K., Clemens, S. C., Rosenthal, Y., Conde, S., Bu, K., Desprat, S., Erb, M., Vetter, L., Franks, M., Cheng, J., Li, L., Liu, Z., Zhou, L. P., Giosan, L., Singh, A., and Mishra, V.: Extreme Indian summer monsoon states stifled Bay of Bengal productivity across the last deglaciation, *Nat. Geosci.*, 18, 443–449, <https://doi.org/10.1038/s41561-025-01684-6>, 2025.
- Ummenhofer, C. C., Gupta, A. S., England, M. H., and Reason, C. J. C.: Contributions of Indian Ocean Sea Surface Temperatures to Enhanced East African Rainfall, *Journal of Climate*, 22, 993–1013, <https://doi.org/10.1175/2008JCLI2493.1>, 2009.
- 910 Ummenhofer, C. C., Kulüke, M., and Tierney, J. E.: Extremes in East African hydroclimate and links to Indo-Pacific variability on interannual to decadal timescales, *Clim Dyn*, 50, 2971–2991, <https://doi.org/10.1007/s00382-017-3786-7>, 2018.
- Vinayachandran, P. N. M., Masumoto, Y., Roberts, M. J., Huggett, J. A., Halo, I., Chatterjee, A., Amol, P., Gupta, G. V. M., Singh, A., Mukherjee, A., Prakash, S., Beckley, L. E., Raes, E. J., and Hood, R.: Reviews and syntheses: Physical and biogeochemical processes associated with upwelling in the Indian Ocean, *Biogeosciences*, 18, 5967–6029, <https://doi.org/10.5194/bg-18-5967-2021>, 2021.
- 915 Wang, Y., Cheng, H., Edwards, R. L., He, Y., Kong, X., An, Z., Wu, J., Kelly, M. J., Dykoski, C. A., and Li, X.: The Holocene Asian Monsoon: Links to Solar Changes and North Atlantic Climate, *Science*, 308, 854–857, <https://doi.org/10.1126/science.1106296>, 2005.
- 920 Wiggert, J. D., Hood, R. R., Banse, K., and Kindle, J. C.: Monsoon-driven biogeochemical processes in the Arabian Sea, *Progress in Oceanography*, 65, 176–213, <https://doi.org/10.1016/j.pocean.2005.03.008>, 2005.
- Yu, W., Xiang, B., Liu, L., and Liu, N.: Understanding the origins of interannual thermocline variations in the tropical Indian Ocean, *Geophysical Research Letters*, 32, <https://doi.org/10.1029/2005GL024327>, 2005.

<https://doi.org/10.5194/egusphere-2026-2343>

Preprint. Discussion started: 24 April 2026

© Author(s) 2026. CC BY 4.0 License.



925 Zheng, X.-T., Xie, S.-P., Du, Y., Liu, L., Huang, G., and Liu, Q.: Indian Ocean Dipole Response to Global Warming in the
CMIP5 Multimodel Ensemble*, *Journal of Climate*, 26, 6067–6080, <https://doi.org/10.1175/JCLI-D-12-00638.1>, 2013.

930